Eclética Química Journal

Volume 44 • number 3 • year 2019

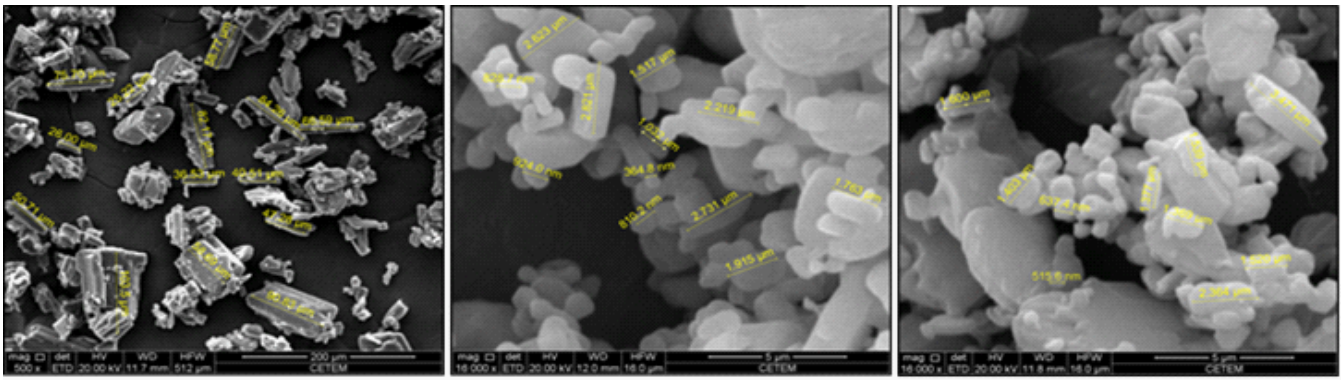

Scanning electron microscopy of the samples NM1, NM2 and NM3 from top to down, with measurements with increase of 500, 20Kv for NM1 and 16.000 X for NM2 and NM3.

Characterization of nimesulide and development of immediate release tablets

Review

Radiopharmaceuticals for diagnosis in nuclear medicine: a short review

Mycology

Diketopiperazines and arylethylamides produced by schizophyllum commune, an endophytic fungus in *Alchornea glandulosa*

Liquid-liquid extraction

Application of a ternary phase diagram to the liquid-liquid extraction of ethanoic acid using ethyl ethanoate

Quantum mechanics

Bound state solution of the Schrödinger equation with inversely quadratic Yukawa/ Attractive Coulomb potential (IQYC) plus Kratzer-Fues (KFP) potential via the WKB quantum formalism

unesp
UNIVERSIDADE ESTADUAL PAULISTA
"JÚLIO DE MESQUITA FILHO"

Instituto de Química
UNESP
Araraquara

ISSN 1678-4618

UNIVERSIDADE ESTADUAL PAULISTA

Reitor

Sandro Roberto Valentini

Vice-reitor

Sergio Roberto Nobre

Pró-reitor de Planejamento Estratégico e Gestão

Leonardo Theodoro Büll

Pró-reitora de Graduação

Gladis Massini-Cagliari

Pró-reitora de Pós-Graduação

Telma Teresinha Berchielli

Pró-reitora de Extensão Universitária

Cleopatra da Silva Planeta

Pró-reitor de Pesquisa

Carlos Frederico de Oliveira Graeff

INSTITUTO DE QUÍMICA

Diretor

Eduardo Maffud Cilli

Vice-Diretora

Dulce Helena Siqueira Silva

Eclética Química Journal

Editorial team
iq.unesp.br/ecletica

| Vol. 44 | n. 3 | 2019 |

Editorial Team

Eclética Química Journal

Editorial
iq.unesp.br/ecletica

| Vol. 44 | n. 3 | 2019 |

Editorial

The Editor proudly announces the third issue of EQJ/2019. In line with the scope of EQJ, readers will find a short review dealing with the main radionuclides and metal complexes currently used as radiopharmaceuticals in nuclear medicine for diagnosis by imaging. Are mentioned those radiopharmaceuticals produced in Brazil together with the more important producers in the country. This issue also brings other interesting subjects as follows: a) characterization of nimesulide raw materials from different manufacturers, development of immediate release tablets and different specification for quality control are described; b) chemical investigation of the crude extract obtained from small-scale and large-scale cultures of the endophytic fungus *Schizophyllum commune*, that resulted in the identification of promising antioxidant, antifungal, and acetylcholinesterase inhibitory activities, being some of compounds identified and isolated by the first time from endophytic fungus of the *Schizophyllum genus*; c) liquid-liquid equilibrium of the extraction process of ethanoic acid in aqueous phase showing good performance of the solvent ethyl ethanoate for concentrations of solute until 16% of the feed; d) theoretical investigation of the bound state solutions of the non-relativistic Schrödinger equation with a mixed potential, using the Wentzel-Kramers-Brillouin quantum theoretical formalism.

The Editor, convinced of the high quality of the articles published so far in EQJ, kindly invite you to submit your manuscript to **Eclética Química Journal** and thanks all authors for their valuable contributions.

Assis Vicente Benedetti
Editor-in-Chief of EQJ

Eclética Química Journal

Author guidelines
iq.unesp.br/ecletica

| Vol. 44 | n. 3 | 2019 |

Instructions for Authors

Preparation of manuscripts

• **Only manuscripts in English will be accepted.** British or American usage is acceptable, but they should not be mixed.

• **The corresponding author should submit the manuscript online**: http://revista.iq.unesp.br/ojs/index.php/ecletica/author

• **Manuscripts must be sent in editable files as** *.doc, *.docx or *.odt. The text must be typed using font style Times New Roman and size 11. Space between lines should be 1.5 mm and paper size A4.

• **The manuscript should be organized in sections as follows:** Introduction, Experimental, Results and Discussion, Conclusions, and References. Sections titles must be written in bold and numbered sequentially; only the first letter should be in uppercase letter. Subsections should be written in normal and italic lowercase letters. For example: **1. Introduction**; *1.1 History;* **2. Experimental**; *2.1 Surface characterization; 2.1.1 Morphological analysis.*

• **The cover letter should include**: the authors' full names, e-mail addresses, ORCID code and affiliations, and remarks about the novelty and relevance of the work. The cover letter should also contain a declaration of the corresponding author, on behalf of the other authors, that the article being submitted is original and its content has not been published previously and is not under consideration for publication elsewhere, that no conflict of interest exists and if accepted, the article will not be published elsewhere in the same form, in any language, without the written consent of the publisher. Finally, the cover letter should also contain the suggestion of 3 (three) suitable reviewers (please, provide full name, affiliation, and e-mail).

• **The first page of the manuscript** should contain the title, abstract and keywords. ***Please, do not give authors names and affiliation, and acknowledgements since a double-blind reviewer system is used. Acknowledgements should be added to the proof only*.**

• **All contributions should include** an Abstract (200 words maximum), three to five Keywords and a Graphical Abstract (8 cm wide and 4 cm high) with an explicative text (2 lines maximum).

• **References should be numbered** sequentially in superscript throughout the text and compiled in brackets at the end of the manuscript as follows:

***Journal*:**

[1] Adorno, A. T. V., Benedetti, A. V., Silva, R. A. G. da, Blanco, M., Influence of the Al content on the phase transformations in Cu-Al-Ag Alloys, Eclet. Quim. 28 (1) (2003) 33-38. https://doi.org/10.1590/S0100-46702003000100004.

***Book*:**

[2] Wendlant, W. W., Thermal Analysis, Wiley-Interscience, New York, 3rd ed., 1986, ch1.

***Chapter in a book*:**

[3] Ferreira, A. A. P., Uliana, C. V., Souza Castilho, M. de, Canaverolo Pesquero, N., Foguel, N. V., Pilon dos Santos, G., Fugivara, C. S., Benedetti, A. V., Yamanaka, H., Amperometric Biosensor for Diagnosis of Disease, In: State of the Art in Biosensors - Environmental and Medical Applications, Rinken, T., ed., InTech: Rijeka, Croatia, 2013, Ch. 12.

***Material in process of publication*:**

[4] Valente Jr., M. A. G., Teixeira, D. A., Lima Azevedo, D., Feliciano, G. T., Benedetti, A. V., Fugivara, C. S., Caprylate Salts Based on Amines as Volatile Corrosion Inhibitors for Metallic Zinc: Theoretical and Experimental Studies, Frontiers in Chemistry. https://doi.org/10.3389/fchem.2017.00032.

• Figures, Schemes, and Tables should be numbered sequentially and presented at the end of the manuscript.

• Nomenclature, abbreviations, and symbols should follow IUPAC recommendations.

• Figures, schemes, and photos already published by the same or different authors in other publications may be reproduced in manuscripts of **Eclet. Quim. J.** only with permission from the editor house that holds the copyright.

• Graphical Abstract (GA) should be a high-resolution figure (900 dpi) summarizing the manuscript in an interesting way to catch the attention of the readers and accompanied by a short explicative text (2 lines maximum). GA must be submitted as *.jpg, *.jpeg or *.tif.

• **Communications** should cover relevant scientific results and are limited to 1,500 words or three pages of the Journal, not including the title, authors' names, figures, tables and references. However, Communications suggesting fragmentation of complete contributions are strongly discouraged by Editors.

• **Review articles** should be original and present state-of-the-art overviews in a coherent and concise form covering the most relevant aspects of the topic that is being revised and indicate the likely future directions of the field. Therefore, before beginning the preparation of a Review manuscript, send a letter (1page maximum) to the Editor with the subject of interest and the main topics that would be covered in Review manuscript. The Editor will communicate his decision in two weeks. Receiving this type of manuscript does not imply acceptance to be published in **Eclet. Quím. J.** It will be peer-reviewed.

• **Short reviews** should present an overview of the state-of-the-art in a specific topic within the scope of the Journal and limited to 5,000 words. Consider a table or image as corresponding to 100 words. Before beginning the preparation of a Short Review manuscript, send a letter (1page maximum) to the Editor with the subject of interest and the main topics that would be covered in the Short Review manuscript.

• **Technical Notes**: descriptions of methods, techniques, equipment or accessories developed in the authors' laboratory, as long as they present chemical content of interest. They should follow the usual form of presentation, according to the peculiarities of each work. They should have a maximum of 15 pages, including figures, tables, diagrams, etc.

• **Articles in Education in Chemistry and chemistry-correlated areas**: research manuscript related to undergraduate teaching in Chemistry and innovative experiences in undergraduate and graduate education. They should have a maximum of 15 pages, including figures, tables, diagrams, and other elements.

• **Special issues** with complete articles dedicated to Symposia and Congresses can be published by **Eclet. Quim. J.** under the condition that a previous agreement with Editors is established. All the guides of the journal must be followed by the authors.

• **Eclet. Quim. J.** Ethical Guides and Publication Copyright:

Before beginning the submission process, please be sure that all ethical aspects mentioned below were followed. Violation of these ethical aspects may prevent authors from submitting and/or publishing articles in **Eclet. Quim. J.**

- The corresponding author is responsible for listing as authors only researchers who have really taken part in the work, and for informing them about the entire manuscript content and for obtaining their permission for submitting and publishing.

- Authors are responsible for carefully searching for all the scientific work relevant to their reasoning irrespective of whether they agree or not with the presented information.

- Authors are responsible for correctly citing and crediting all data used from works of researchers other than the ones who are authors of the manuscript that is being submitted to **Eclet. Quim. J.**

- Citations of Master's Degree Dissertations and PhD Theses are not accepted; instead, the publications resulting from them must be cited.

- Explicit permission of a non-author who has collaborated with personal communication or discussion to the manuscript being submitted to **Eclet. Quím. J.** must be obtained before being cited.

- Simultaneous submission of the same manuscript to more than one journal is considered an ethical deviation and is conflicted to the declaration has been done below by the authors.

- Plagiarism, self-plagiarism, and the suggestion of novelty when the material was already published are unaccepted by **Eclet. Quim. J.**

- The word-for-word reproduction of data or sentences as long as placed between quotation marks and correctly cited is not considered ethical deviation when indispensable for the discussion of a specific set of data or a hypothesis.

- Before reviewing a manuscript, the *turnitin* anti-plagiarism software will be used to detect any ethical deviation.

- The corresponding author transfers the copyright of the submitted manuscript and all its versions to **Eclet. Quim. J.**, after having the consent of all authors, which ceases if the manuscript is rejected or withdrawn during the review process.

- Before submitting manuscripts involving human beings, materials from human or animals, the authors need to confirm that the procedures established, respectively, by the institutional committee on human experimentation and Helsinki's declaration, and the recommendations of the animal care institutional committee were followed. Editors may request complementary information on ethical aspects.

- When a published manuscript in EQJ is also published in other Journal, it will be immediately withdrawn from EQJ and the authors informed of the Editor decision.

• Manuscript Submissions

For the first evaluation: the manuscripts should be submitted in three files: the cover letter as mentioned above, the graphical abstract and the entire manuscript.

The entire manuscript should be submitted as *.doc, *.docx or *.odt files.

The Graphical Abstract (GA) 900 dpi resolution is mandatory for this Journal and should be submitted as *.jpg, *.jpeg or *.tif files as supplementary file.

The cover letter should contain the title of the manuscript, the authors' names and affiliations, and the relevant aspects of the manuscript (no more than 5 lines), and the suggestion of 3 (three) names of experts in the subject: complete name, affiliation, and e-mail).

• Reviewing

The time elapsed between the submission and the first response of the reviewers is around 3 months. The average time elapsed between submission and publication is 7 months.

• **Resubmission** (manuscripts "rejected in the present form" or subjected to "revision"): **A LETTER WITH THE RESPONSES TO THE COMMENTS/CRITICISM AND SUGGESTIONS OF REVIEWERS/EDITORS SHOULD ACCOMPANY THE REVISED MANUSCRIPT. ALL MODIFICATIONS MADE TO THE ORIGINAL MANUSCRIPT MUST BE HIGHLIGHTED.**

• Editor's requirements

Authors who have a manuscript accepted in **Eclética Química Journal** may be invited to act as reviewers.

Only the authors are responsible for the correctness of all information, data and content of the manuscript submitted to **Eclética Química Journal**. Thus, the Editors and the Editorial Board cannot accept responsibility for the correctness of the material published in **Eclética Química Journal**.

• Proofs

After accepting the manuscript, **Eclet. Quim. J.** technical assistants will contact you regarding your manuscript page proofs to correct printing errors only, i.e., other corrections or content improvement are not permitted. The proofs shall be returned in 3 working days (72 h) via e-mail.

• Authors Declaration

The corresponding author declares, on behalf of the other authors, that the article being submitted is original and has been written by the stated authors who are all aware of its content and approve its submission. Declaration should also state that the article has not been published previously and is not under consideration for publication elsewhere, that no conflict of interest exists and if accepted, the article will not be published elsewhere in the same form, in any language, without the written consent of the publisher.

• Appeal

Authors may only appeal once about the decision regarding a manuscript. To appeal against the Editorial decision on your manuscript, the corresponding author can send a rebuttal letter to the editor, including a detailed response to any comments made by the reviewers/editor. The editor will consider the rebuttal letter, and if dimmed appropriate, the manuscript will be sent to a new reviewer. The Editor decision is final.

• Contact

Gustavo Marcelino de Souza (ecletica@journal.iq.unesp.br)

Submission Preparation Checklist

As part of the submission process, authors are required to check off their submission's compliance with all of the following items, and submissions may be returned to authors that do not adhere to these guidelines.

In **Step 1**, select the appropriate section for this submission.

Be sure that Authors' names, affiliations and aknowledgements were removed from the manuscript. The manuscript must be in *.doc, *.docx or *.odt format before uploading in **Step 2**.

In **Step 3**, add the full name of each author including the ORCID IDs in its full URL ONLY WITH HTTP, NOT HTTPS (eg. http://orcid.org/0000-0002-1825-0097).

Add the authors in the same order as they appear in the manuscript in **step 3**.

Be sure to have the COVER LETTER and GRAPHICAL ABSTRACT (according to the Author Guildelines) to upload them in **Step 4**.

Check if you've followed all the previous steps before continuing the submission of your manuscript.

Copyright Notice

The corresponding author transfers the copyright of the submitted manuscript and all its versions to **Eclet. Quim. J.**, after having the consent of all authors, which ceases if the manuscript is rejected or withdrawn during the review process.

Self-archive to institutional, thematic repositories or personal web page is permitted just after publication.

Eclética Química Journal

Summary
iq.unesp.br/ecletica

| Vol. 44 | n. 3 | 2019 |

SUMMARY

Eclética Química Journal

Short review
iq.unesp.br/ecletica

| Vol. 44 | n. 3 | 2019 |

Radiopharmaceuticals for diagnosis in nuclear medicine: a short review

Filipe Boccato Payolla[1], Antonio Carlos Massabni[1,2+], Chris Orvig[3]

1 University of Araraquara (Uniara), 1217 Carlos Gomes St., Araraquara, São Paulo, Brazil
2 São Paulo State University (Unesp), Institute of Chemistry, 55 Professor Francisco Degni St., Araraquara, São Paulo, Brazil
3 University of British Columbia (UBC), Faculty of Pharmaceutical Sciences, Department of Chemistry, Medicinal Inorganic Chemistry Group, 2405 Wesbrook Mall, Vancouver, British Columbia, Canada

[+]Corresponding author: Antonio Carlos Massabni, email address: amassabni@uol.com.br

ARTICLE INFO

Article history:
Received: January 30, 2019
Accepted: June 29, 2019
Published: July 4, 2019

Keywords:
1. radionuclide
2. nuclear medicine
3. diagnosis
4. radiopharmaceutical

ABSTRACT: Radiopharmaceuticals are radioactive compounds which have a bound radionuclide in their structure, whose purpose is directing the radionuclide to a location to be treated or to obtain images. Nuclear medicine is the medical specialty that employs radiopharmaceuticals, which has presented itself as a tremendously useful ally for medicine assisting in various diagnoses and treatments, especially for cancer. The general objective of this work is to identify the main radionuclides and metal complexes currently used as radiopharmaceuticals. The main metal complexes used as radiopharmaceuticals are compounds of technetium (^{99m}Tc) like sodium pertechnetate and methylenediphosphonate MDP-^{99m}Tc and other compounds of indium (^{111}In), thallium (^{201}Tl), gallium (^{67}Ga, ^{68}Ga), iodine (^{123}I and ^{131}I), chromium (^{51}Cr), sulphur (^{35}S), phosphorus (^{32}P), fluorine (as fluorodeoxyglucose, ^{18}F-FDG and sodium fluorine, Na^{18}F), which are widely used in the nuclear medicine for diagnosis by imaging. They have been of great importance for the early diagnosis of numerous diseases, mainly cancer.Currently, technetium compounds are the majority of radiopharmaceuticals used in all countries. In Brazil, Institute of Energy and Nuclear Research (IPEN) is one of the most important distributors of radiopharmaceuticals, producing, importing and distributing them to clinics and hospitals over the country.

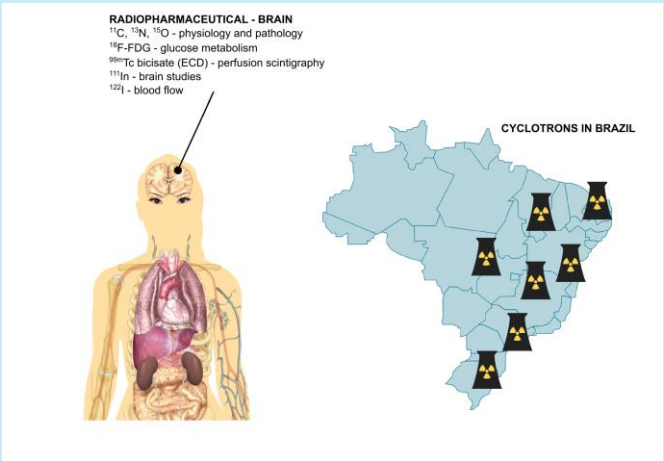

CONTENTS

1. Introduction

In nuclear medicine, radiopharmaceuticals are used in diagnostic imaging and radiotherapy, being of utmost importance for medicine in general to assist in diagnoses of organs and treatments of pathological conditions, especially cancer. In the imaging modality, radiopharmaceuticals are administered via oral, intravenous, or by inhalation

to enable visualization with their radioactive tracers of various organs, such as kidneys, lungs, thyroid and heart functions, bone metabolism and blood circulation. In therapeutic modality, aiming to treat cancer or over functioning thyroid gland, a high dose of radiation is delivered through specific radiopharmaceuticals targeting the diseased organ[1].

Radiopharmaceuticals generally consist of two components, a radioactive element (radionuclide), that permits external scan, linked to a non-radioactive element, a biologically active molecule, drug or cell (red and white blood cells labeled with a radionuclide, for example) that acts as a carrier or ligand, responsible for conducting the radionuclide to a specific organ[2].

Some characteristics are necessary for considering radiopharmaceuticals clinically useful for imaging: the decay of the radionuclide should be in specific ranges of energy emissions (511 keV for positron emission tomography – PET and 100-200 keV for gamma cameras) and in sufficient quantity for tomography detection; 2) it should not contain particulate radiation (beta emissions, for example), because it increases the radiation dose in patients; 3) the half-life should be for a few hours only; 4) the radionuclides should not be contaminated by other radionuclides of the same element nor even its stable radionuclides (carrier-free); 5) they should have specific activity, and the highest specific activity comes from carrier-free radionuclides; 6) the radiopharmaceutical should not have toxicity and does not manifest physiological effects; 7) the radiopharmaceutical should be available for instant usage and easy to compound; 8) the radiopharmaceutical should reach the target organ quickly and accurately, according to its intended application[3].

Diagnostic radiopharmaceuticals have no pharmacological effects and their administration is not associated with relevant clinical side effects. Its clinical use, however, carries the inherent risk of exposure to radiation and possible contamination during radiopharmaceutical formulation, since most radiopharmaceuticals are administered intravenously[3].

The most notable difference between normal medicines and radiopharmaceuticals is that the former has therapeutic effect while the latter does not. Besides that, radiopharmaceuticals have a short half-life, because of their rapid decay. For this reason, radiopharmaceuticals must be prepared immediately before their administration. The preparation and use of radiopharmaceuticals with safety and expertise are therefore vital for operator and patient protection[3].

Understanding the mechanism of interaction between the radioactive elements and the different molecules, drugs, cells and organs it is necessary for the development of more efficient imaging or therapeutic radiopharmaceuticals[4].

2. Historical Bases of Nuclear Medicine and Radioactivity

Wilhelm Roentgen's work on X-ray studies has stimulated researchers such as Henri Poincaré whose studies are related to the hypothesis of X-ray emission and fluorescence. The first scientist to carry out the hypotheses proposed by Poincaré was Charles Henry, using zinc sulfide as an X-ray intensifier, concluding that in the presence of light, when the radiographs became sharper because of the substance[5].

In 1896, Henri Becquerel used uranium salts on photographic plates, which resulted in marked radiographs without the presence of light. In 1905, Marie and Pierre Curie were the first to suggest radium for treatment of cancer. The Curies' work may be considered the beginning of modern nuclear medicine. In 1931, Ernest Lawrence built the first cyclotron, equipment that accelerated alpha particles, such as protons, deuterons, or helium ions, with the aim of penetrating the nucleus to produce stable and radioactive isotopes. A decade later, Lawrence's cyclotron had produced 223 radioactive isotopes, many of which are now of great value for medicinal uses and studies in the biological sciences[6].

In 1930, Ernest Lawrence and Milton Livingstone, with their invention of the cyclotron, allowed the artificial production of new radioactive elements, but the quantities were very small. The medical use of radionuclides began during World War II with the Oak Ridge reactor in the United States, initiating the production of radionuclides in global scale. Hal Anger, in 1958, developed the image-scintillation chamber, which did not require the movement of the detector. It had a higher geometric resolution, and it was possible to obtain different projections of the same distribution of the radiopharmaceutical. However, computers were not yet capable of acquiring the information and transforming it into images. So, the information was sent to the cathode ray tube for it to be recorded on photographic plates or films. The modern

Eclética Química Journal, vol. 44, n. 3, 2019, 11-19
ISSN: 1678-4618
DOI: 10.26850/1678-4618eqj.v44.3.2019.p11-19

scintillation cameras used nowadays are the Anger camera type[7].

Nuclear Medicine only had a diagnostic power when Paul Harper and his group introduced the ^{99m}Tc radionuclide as a marker. This radionuclide decays by isometric transition emitting photon with energy of 140 keV, gamma-type radiation and physical half-life of about 6 hours, which allows studies with reasonable intervals. In addition, it is obtained by the decay of the parent element ^{99}Mo, produced in ^{99}Mo/^{99m}Tc generators[7].

The first radiopharmaceuticals were commercialized in 1950. ^{131}Iodine was the first commercially available isotope, with Abbott Laboratories being the first company to produce radiopharmaceuticals for medical uses[8].

The radioactive elements, thus classified, may have highly energetic unstable nuclides due to the excess of energy, which stabilizes by the emission of particles or electromagnetic radiation or charged particles during radioactive decay. In this context, there are three types of radiation: alpha, beta minus and gamma[1,2]. Radiation propagates at a certain speed and contains energy with electric and magnetic charges that can be generated by natural sources or by artificial devices, such as a cyclotron. Ionizing radiation is generated from the energy emitted by an unstable nucleus in artificial form or by a cyclotron[5].

3. Nuclear Medicine and Radiopharmaceuticals

Radiopharmaceuticals may be divided in two distinct groups: one that includes radionuclides with radioactive decay period (half life) less than 2 h, and other that includes radionuclides with half life higher than 2 h[9].

Nuclear medicine cameras are proper for identifying radioactive particles. The type of radiation emitted defines the type of camera: SPECT cameras are used to detect nuclides that decay through direct emission of single gamma rays, and PET cameras are able to detect the pair of gamma rays emitted after a decay of positron[10].

3.1 Nuclear medicine techniques

Diagnostic techniques in nuclear medicine use radioactive tracers that emit gamma radiation from within the body. The camera constructs an image from the points where the radiation is emitted. This image is magnified on a computer and it can be observed on a monitor that indicates the anomalies[11].

The nuclear medicine techniques include Single Photon Emission Computerized Tomography (SPECT), Positron Emission Tomography (PET), and computed tomography-PET (PET-CT) (for better anatomical visualization), micro-PET (with ultra-high resolution) and microcomputerized axial tomography micro-CAT. These techniques are used to analyze biochemical dysfunctions as early signs of the disease, its mechanisms and association with disease states from cancer to cardiovascular diseases and mental disorders[6,12].

A SPECT exam is used primarily to visualize the blood flow through veins and arteries, and to perform pre-surgical evaluation of seizures. SPECT is also useful in the diagnosis of blood deprived areas of brain (ischemic), spinal stress fractures (spondylolysis) and tumors[10].

The PET imaging detects the pair of gamma rays produced by the interaction between a positron and an electron in the tissues of the body. The electron and the positron neutralize each other producing two gamma rays in opposite directions. PET detects the electronic signal converting with scintillation crystals the energy released by gamma rays[10].

^{99m}Technetium is the radionuclide that has the best characteristics to combine with gamma cameras and ^{18}fluorine has the most desirable characteristics for PET[3].

Although the SPECT and PET techniques capture images with high intensity, they have low spatial resolution because they are directed to the surface of the body they are accurately visualized. On the other hand, computerized tomography (CT) and magnetic resonance have greater spatial resolution, but with less sensitivity. To obtain such restrictions, the techniques are merged for images with excellent spatial resolution combined with high sensitivity[10].

X-ray CT has a computational process that makes a three-dimensional image, resulting in images with much greater resolution and quantity of details of internal structures and organs of the body[6]. There are other non-nuclear techniques, which are not described in this review, but could be accessed in this reference[10].

3.2. Radionuclides in medicine

Radionuclides have many applications in several areas that use nuclear technology. The use

Eclética Química Journal, vol. 44, n. 3, 2019, 11-19
ISSN: 1678-4618
DOI: 10.26850/1678-4618eqj.v44.3.2019.p11-19

of radiation and radionuclides in medicine is continuously increasing both for diagnosis and therapy worldwide.

In developed countries (1/4 of the world's population), one person in 50 is subject to nuclear medicine and the frequency of radionuclide therapy is about 10% of that number, according to the World Nuclear Association[11].

Radiation is used in nuclear medicine to obtain information about the organs of a person for treatment of a disease. In many cases, information is used for a quick diagnosis. Thyroid, bones, heart, liver, kidney and many other organs can be easily observed in the generated image and the anomalies of its functions are revealed. About 10,000 hospitals worldwide use radionuclides and about 90% of the procedures are for diagnosis. The radionuclide most used in diagnostics is ^{99m}Tc. It has been used in about 40 million exams per year, which means 80% of all exams in nuclear medicine worldwide[11].

Radionuclides are essential components of diagnostic exams. In combination with the equipment recording the images from the emitted gamma rays, the processes that occur in various parts of the body can be studied. For diagnosis, a dose of the radioactive material is given to the patient and the localization in the organ can be studied as a two-dimensional image or, using tomography, as a three-dimensional image. These gamma or positron tracers have short-lived isotopes and are linked to chemical compounds that allow specific physiological processes to be evaluated[10,11].

In the USA, more than 20 million medical applications per year are performed using radionuclides and in Europe about 10 million per year[11]. In Brazil, the Nuclear and Energy Research Institute (IPEN) reported that, in 2017, there were 360 diagnostic clinics and nuclear medicine hospitals, 70% in the South and Southeast regions of Brazil, 72 PETs installed, others to be licensed, 33 hospitals with rooms for therapy and approximately 1.8 million patients per year[14].

3.3 Radiopharmaceuticals for diagnosis in human body

Medical doctors and chemists have identified a large number of chemicals that are absorbed by specific organs. Thyroid, for example, absorbs iodine while the brain absorbs glucose. Diagnostic radiopharmaceuticals can be used to monitor blood flow to the brain, liver, lung, heart, and kidney[14].

Particulate radiation can be useful for destroying or weakening cancer cells (radiotherapy). The radionuclide that generates the radiation can be located in a certain organ in the same way used for diagnostics. In many cases, beta radiation causes the destruction of cancer cells. ^{177}Lutetium (^{177}Lu), for example, is prepared from ^{176}ytterbium (^{176}Yb) which is irradiated to transform it into ^{177}Yb, which rapidly returns to ^{177}Lu. ^{90}Yttrium (^{90}Y) is used to treat cancer, especially non-Hodgkin's lymphoma and liver cancer. ^{131}Iodine (^{131}I), ^{153}samarium (^{153}Sm) and ^{32}phosphorus (^{32}P) are also used in radiotherapy. ^{131}Cesium (^{131}Cs), ^{103}palladium (^{103}Pd) and ^{223}radium (^{223}Ra) are used in special cases[11].

Figure 1 lists the radionuclides most commonly used for diagnosis and treatment of different organs of the human body.

Eclética Química Journal, vol. 44, n. 3, 2019, 11-19
ISSN: 1678-4618
DOI: 10.26850/1678-4618eqj.v44.3.2019.p11-19

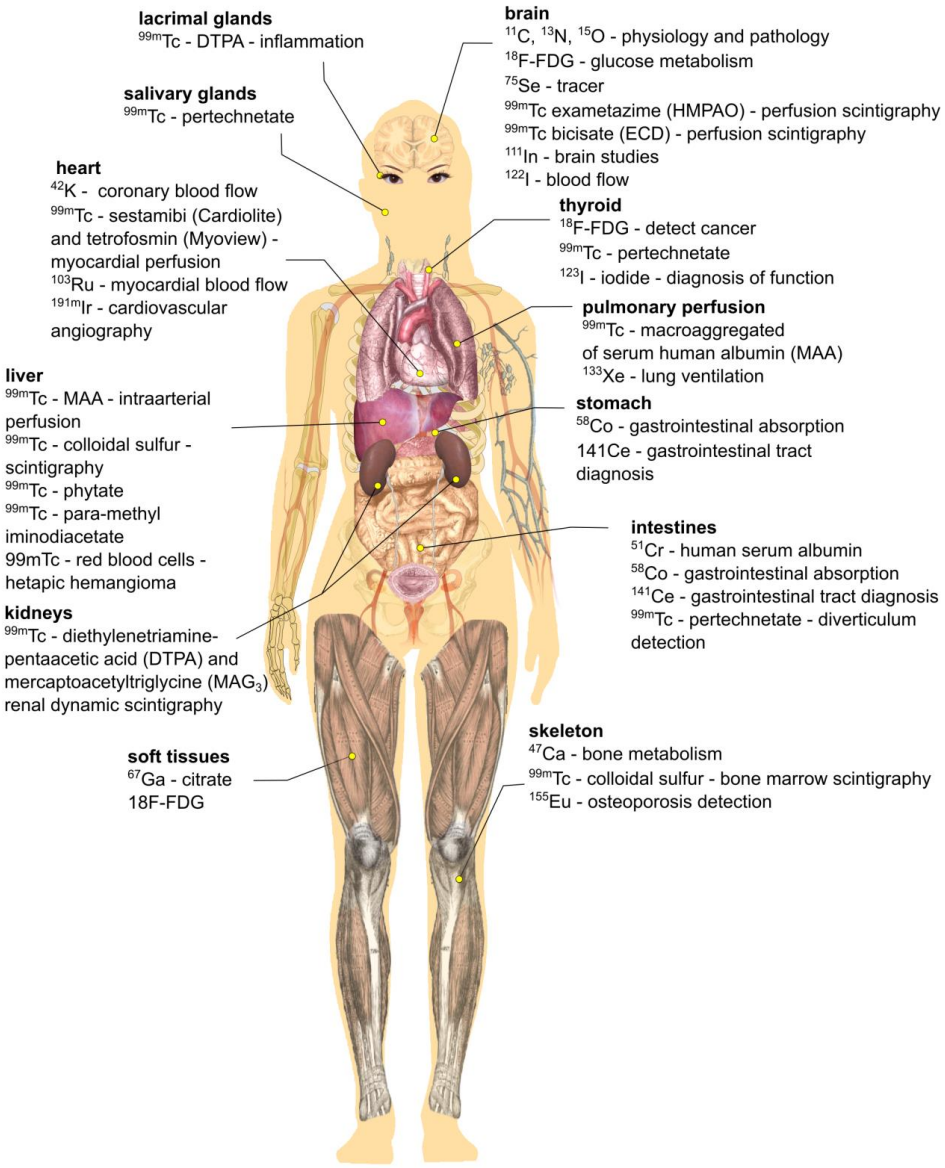

Figure 1. Different radiopharmaceuticals and target organs for imaging[4,13,14]. *Image released into the public domain, changed for the review purposes*[15].

4. Production of radionuclides

Radionuclides found in nature, such as uranium and radium, are heavy elements with high toxicity and long half-life (over 1,000 years), so they are not used clinically. Radionuclides used in nuclear medicine are artificially produced by neutron bombardment or nuclear fission[4].

Many radionuclides are produced in nuclear reactors and cyclotrons. Generally, neutron-rich radioisotopes and those resulting from nuclear fission are produced in reactors (Table 1) and the neutron-poor radioisotopes are produced in cyclotrons (Table 2). There are about 30 radioisotopes produced by activation and 5 are reactor melt products. A list with 70 elements, their isotopes, half-lives, decay, main energy and applications can be found in the reference[14].

Eclética Química Journal, vol. 44, n. 3, 2019, 11-19
ISSN: 1678-4618
DOI: 10.26850/1678-4618eqj.v44.3.2019.p11-19

Table 1. 30 selected radionuclides produced by nuclear fission[14].

^{213}bismuth	^{59}iron	^{153}samarium
^{131}caesium	^{212}lead	^{75}selenium
^{137}caesium	^{177}lutetium	^{24}sodium
^{51}chromium	^{99}molybdenum	^{89}strontium
^{60}cobalt-60	^{103}palladium	^{99m}technetium
^{165}dysprosium	^{32}phosphorus	^{227}thorium
^{169}erbium	^{42}potassium	^{133}xenon
^{166}holmium	^{223}radium	^{169}ytterbium
^{131}iodine	^{186}rhenium	^{177}ytterbium
^{192}iridium	^{188}rhenium	^{90}yttrium

Table 2. 18 selected radionuclides produced by cyclotrons[14].

^{225}actinium	^{67}copper
^{211}astatine	^{67}gallium
^{213}bismuth	^{127}xenon
^{11}carbon	^{111}indium
^{13}nitrogen	^{123}iodine
^{15}oxygen	^{124}iodine
^{18}fluorine	^{81m}krypton
^{57}cobalt	^{82}rubidium
^{64}copper	^{201}thallium

In Brazil, the main producer of radiopharmaceuticals is IPEN, located in the city of São Paulo, state of São Paulo. IPEN is the only producer in the country of the ^{99m}technetium generator, which is used in 80% of the nuclear medicine procedures in Brazil. IPEN is also responsible for the production of 38 radiopharmaceuticals with distribution for all the Brazilian states[13]. According to data from the National Commission for Nuclear Energy (CNEN) Management Report for 2017, published in August 2018, about the radiopharmaceutical industry in Brazil, the main producers of radiopharmaceuticals are: Nuclear and Energy Research Institute (IPEN – São Paulo), Nuclear Technology Development Center (CDTN – Belo Horizonte), Northeast Regional Center for Nuclear Sciences (CRCN-NE – Recife), Nuclear Engineering Institute (IEN – Rio de Janeiro) operating nuclear reactors and particle accelerators, producing and commercializing supplies for the medical area. The Institute of Radiation Protection and Dosimetry (IRD – Rio de Janeiro) and the Laboratory of Poços de Caldas (LAPOC – Poços de Caldas) are research laboratories that provide services to other laboratories, industries and companies and do not produce radiopharmaceuticals[13].

The constitutional amendment 49 published in February 9, 2006 defines that production, commercialization and use of radionuclides with a half-life less than or equal to two hours are authorized and commercialization and use of radionuclides for research and medical, agricultural and industrial uses[14].

Table 3 shows the radiopharmaceuticals produced in Brazil and places where they are manufactured.

Table 3. Radiopharmaceuticals produced in Brazil[13].

Product	**Place of production**
sodium iodide (^{123}I)	IEN
sodium iodide (^{131}I)	IPEN
gallium citrate (^{67}Ga)	IPEN
thallium chloride (^{201}Tl)	IPEN
sodium chromate (^{51}Cr)	IPEN
generator ^{99}Mo – ^{99m}Tc	IPEN
sodium sulfate (^{35}S)	IPEN
phosphoric acid (^{32}P)	IPEN
sodium phosphate (^{32}P)	IPEN
^{18}fluorodeoxyglucose (^{18}F-FDG)	IPEN, IEN, CDTN, CRCN-NE
EDTMP (^{153}Sm)	IPEN
sodium fluoride (Na^{18}F)	IPEN, CDTN
^{111}indium (^{111}In)	IPEN
dotatate (^{177}Lu)	IPEN

In addition to these radiopharmaceuticals, CNEN supplies sealed sources (^{133}Ba, ^{137}Cs and ^{57}Co), ^{192}Ir and ^{125}I seeds, both used in oncological treatments, using brachytherapy procedures[13].

Production of technetium in Brazil still depends on raw material from foreign origin (^{99}molybdenum), and on the costs of importation. However, within the next few years, the CNEN aims at implementing the Brazilian Multipurpose Reactor (RMB) in the city of Iperó, state of São Paulo. Also, the Federal Government plans to initiate RMB's usage in 2024, becoming independent and guaranteeing the nationalization of the ^{99}molybdenum radionuclide for the country's

Eclética Química Journal, vol. 44, n. 3, 2019, 11-19
ISSN: 1678-4618
DOI: 10.26850/1678-4618eqj.v44.3.2019.p11-19

demand[16,17]. This reactor must produce *circa* 1,000 Ci of ^{99}Mo per week (Ci (*curie*) is a unit of radionuclide activity, defined as: 1 Ci = 3,7 × 10^{10} disintegrations per second[20]). As a comparison, in 2014, national demand was 450 Ci ^{99}Mo/week[17,18]; the worldwide demand, in 2018, was 9 400 Ci ^{99}Mo/week[19].

Figure 2 shows all cyclotrons installed and in operation in Brazil in 2019.

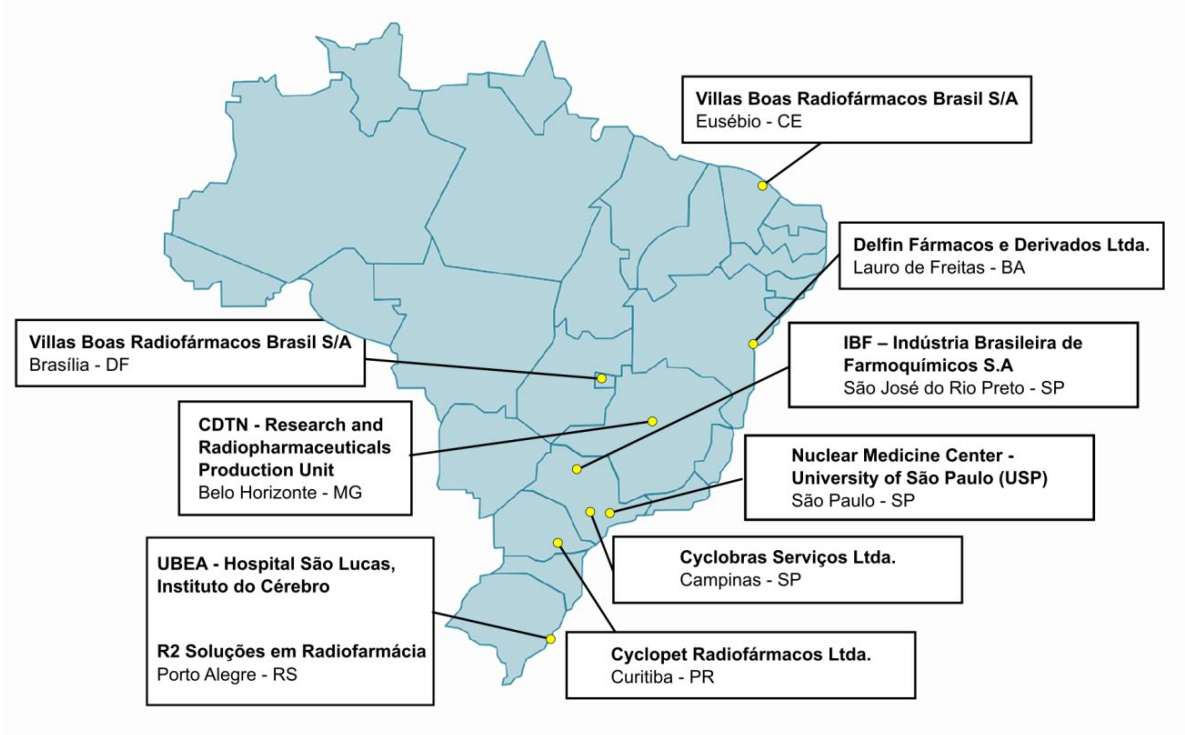

Figure 2. Cyclotron installations in Brazil[21]. *Image released into the public domain, changed for the review purposes*[22].

The main difficulties for production of new radiopharmaceuticals in Brazil are the lack of a 70 MeV high energy cyclotron accelerator in the country and the adequacy of the facilities to follow the Brazilian National Sanitary Surveillance Agency (Anvisa) Resolution nº 63[14].

5. Conclusions

Radionuclides have many applications in several areas which use nuclear energy. The importance and uses of radionuclides in medicine is continuously increasing for diagnosis and therapy worldwide. In 2018, about 10,000 hospitals used radionuclides and about 90% of the procedures were for diagnosis. In Brazil, the Institute of Energy and Nuclear Research (IPEN) reported that in 2017 there were more than 440 diagnostic clinics and nuclear medicine hospitals, 55% in the Southeast region of Brazil, 19% in Northeast and 15% in South region; 72 PETs installed, with about 1.8 million people supported. There are about 40 radionuclides produced in nuclear reactors and about 20 radionuclides produced in cyclotrons.

^{99m}Technetium is the most used radionuclide for diagnosis, accounting for 67.3% of total CNEN revenue in 2017. Besides ^{99m}Tc, ^{131}I (13.7%), ^{67}Ga (2.9%), ^{177}Lu Dotatate (2.9%) and ^{18}F-FDG (1.1%) were more frequently used in Brazil in 2017.

SPECT and PET are the two most used techniques in nuclear medicine during a large period, but nowadays other techniques with more accurate results are emerging, among them X-ray computed tomography e with three-dimension images.

6. Acknowledgements

The authors thank the support from São Paulo Research Foundation (FAPESP Proc. nº 2017/11570-3).

Eclética Química Journal, vol. 44, n. 3, 2019, 11-19
ISSN: 1678-4618
DOI: 10.26850/1678-4618eqj.v44.3.2019.p11-19

7. References

[1] World Health Organization (WHO). Diagnostic imaging. Nuclear Medicine. https://www.who.int/diagnostic_imaging/imaging_modalities/dim_nuclearmed/en/.

[2] Cherry, S. R., Sorenson, J. A., Phelps, M. E. Physics in Nuclear Medicine. Elsevier Inc. ISBN 978-1-4160-5198-5 2012. https://www.sciencedirect.com/topics/neuroscience/radiopharmaceuticals.

[3] International Atomic Energy Agency (IAEA). Operational guidance on hospital radiopharmacy : a safe and effective approach. Vienna: International Atomic Energy Agency, 2008. ISBN 978-92-0-106708-1. https://www-pub.iaea.org/MTCD/publications/PDF/Pub1342/Pub1342_web.pdf.

[4] Ziessman, H. A., O'Malley, J. P., Thrall, J. H. (eds.). Radiopharmaceuticals, In: Nuclear Medicine, 4th ed., W. B. Saunders: Philadelphia, USA, 2014, ch. 1. ISBN 9780323082990. https://doi.org/10.1016/B978-0-323-08299-0.00001-8.

[5] Malley, M. C., Radioactivity: a history of a mysterious science, Oxford University Press, New York, 2011, ISBN 978-0-19-976641-31.

[6] L'Annunziata, M. F., Radioactivity: introduction and history, from the quantum to quarks, Elsevier, 2nd ed., 2016. eBook ISBN: 9780444634962.

[7] Robilotta, C. C., A tomografia por emissão de pósitrons: uma nova modalidade na medicina nuclear brasileira, Rev. Panam. Salud Pública 20 (2/3) (2006) 134-42. https://doi.org/10.1590/S1020-49892006000800010.

[8] Santos-Oliveira, R., Carneiro-Leão, A. M. A., A história da radiofarmácia e as implicações da Emenda Constitucional nº 49. Rev. Bras. Cienc. Farm. 44 (3) 2008. http://qnesc.sbq.org.br/online/cadernos/06/a08.pdf.

[9] Comissão Nacional de Energia Nuclear (CNEN), RMB e a Produção de Radiofármacos. http://www.cnen.gov.br/radiofarmacos.

[10] Wells, R. G., Instrumentation in molecular imaging. J. Nucl. Cardiol. 23 (6) 2016, 1343-1347. https://doi.org/10.1007/s12350-016-0498-z.

[11] World Nuclear Association (WNA). Radionuclides in medicine. (Updated November 2018). http://www.world-nuclear.org/information-library/non-power-nuclear-applications/radionuclides-research/radionuclides-in-medicine.aspx.

[12] K, Seyed. Molecular Nuclear Imaging: The Radiopharmaceuticals (Review) .Cancer Biotherapy and Radiopharmaceuticals, 20 (2) 2005. https://doi.org/10.1089/cbr.2005.20.163.

[13] Comissão Nacional de Energia Nuclear (CNEN), Ministério da Ciência, Tecnologia, Inovação e Comunicações, Relatório de Gestão do exercício de 2017. http://www.cnen.gov.br/images/cnen/documentos/acesso_a_informacao/Rel-gestao-2017.pdf.

[14] European Organization for Nuclear Research (CERN), A table of frequently used radioisotopes – CERN Document Server. C. Grupen, Introduction to Radiation Protection, Graduate Texts in Physics, 2010. https://doi.org/10.1007/978-3-642-02586-0.

[15] Wikimedia Commons, the free media repository, 'File: Female shadow template.svg'. https://commons.wikimedia.org/w/index.php?title=File:Female_shadow_template.svg&oldid=302058264.

[16] Amazônia Azul Tecnologias de Defesa S.A. (Amazul), Reator Multipropósito Brasileiro. https://www.marinha.mil.br/amazul/acesso-a-informacao/acoes-e-programas/programas/reator-multiproposito-brasileiro.

[17] Instituto de Pesquisas Energéticas e Nucleares (IPEN). Brazilian Multipurpose Reactor – Progress Report. 6 p. 2016. https://www.ipen.br/portal_por/conteudo/documentos/PR_2014_2016_13_Brazilian_Multipurpose_Reactor.pdf.

[18] Pozzo, L., Coura Filho, G., Osso Júnior, J. A., Squair, P. L., SUS in nuclear medicine in Brazil: analysis and comparison of data provided by Datasus and CNEN, Radiol. Bras., 47 (3) (2014) 141-148. https://doi.org/10.1590/0100-3984.2013.1906.

[19] Nuclear Energy Agency (NEA), Steering Committee For Nuclear Energy, High-Level Group on the Security of Supply of Medical Radioisotopes, The supply of medical radioisotopes – 2018 medical isotope demand and capacity projection for the 2018-2023 period. http://www.oecd.org/officialdocuments/publicdisplaydocumentpdf/?cote=NEA/SEN/HLGMR(2018)3&docLanguage=En.

[20] International Atomic Energy Agency (IAEA). Activity measurement principles.

Eclética Química Journal, vol. 44, n. 3, 2019, 11-19
ISSN: 1678-4618
DOI: 10.26850/1678-4618eqj.v44.3.2019.p11-19

https://humanhealth.iaea.org/HHW/MedicalPhysics/NuclearMedicine/ActivityMeasurements/ActMeasPrinciples/index.html.

[21] Comissão Nacional de Energia Nuclear (CNEN), Instalações Autorizadas. Produção de Radioisótopos (Cíclotron) – Posição em 02/06/2019. http://appasp.cnen.gov.br/seguranca/cons-ent-prof/lst-entidades-aut-cert.asp?p_ent=22&d=Produção de Radioisótopos (Ciclotron).

[22] Pixabay. 'File: brazil-23553_960_720.png'. Pixabay, 2 Apr. 2012. Available from: https://pixabay.com/pt/vectors/brasil-mapa-américa-do-sul-estados-23553/.

Eclética Química Journal, vol. 44, n. 3, 2019, 11-19
ISSN: 1678-4618
DOI: 10.26850/1678-4618eqj.v44.3.2019.p11-19

Eclética Química Journal

Original article
iq.unesp.br/ecletica

| Vol. 44 | n. 3 | 2019 |

Characterization of nimesulide and development of immediate release tablets

Helvécio Vinícius Antunes Rocha+, Rachel de Sousa Augusto, Livia Deris Prado, Erika Martins de Carvalho

Oswaldo Cruz Foundation (Fiocruz), Institute of Technology in Drugs, 4365 Brasil Av., Manguinhos, Rio de Janeiro, Brazil

+Corresponding author: Helvécio Vinícius Antunes Rocha, email address: helvecio.far@gmail.com

ARTICLE INFO

Article history:
Received: December 22, 2018
Accepted: March 30, 2019
Published: July 4, 2019

Keywords:
1. nimesulide
2. raw material characterization
3. dissolution profile
4. powder flow
5. formulation development

ABSTRACT: This paper aims to characterize nimesulide raw materials from different manufacturers and to develop immediate release tablets, in order to register a generic product. Also, raw material characteristics and the tablets final properties were investigated in order to establish a different specification for quality control. Two micronized and one non-micronized nimesulide samples were obtained from different manufacturers and were characterized by thermal analysis, spectroscopic techniques, morphological analysis, flowability and biopharmaceutical evaluation. The samples belong to the same polymorph. The formulations design and the choice of the production process were carried out based on the results obtained in the characterization assessments. The proposed formulations showed different dissolution behavior. One formulation was selected and then the dissolution was evaluated in different dissolution media containing varying concentrations of surfactant, in order to verify if the concentration of 2% (v/v) of polysorbate 80, recommended by the Brazilian Pharmacopoeia, would be overestimating the bioavailability of the drug. The results showed that the percentage of surfactant present in the dissolution medium directly impacts the amount of dissolved drug. The selected formulation demonstrated promising results to proceed with the bio batches manufacture and the pharmaceutical equivalence study.

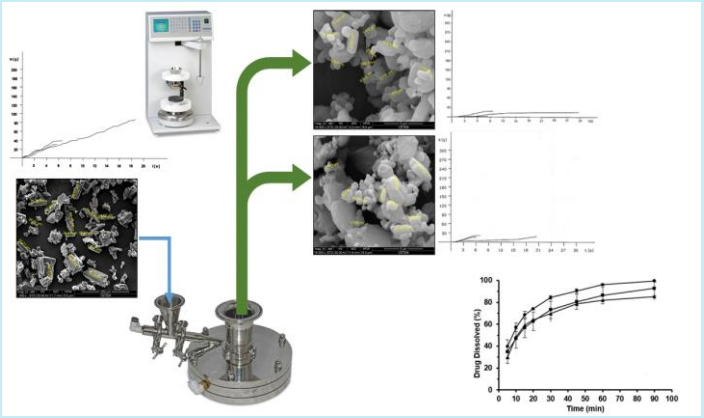

1. Introduction

Nimesulide is a nonsteroidal sulfonamide and belongs to the class of anti-inflammatory drugs (NSAIDs) that demonstrates a selectivity for COX-2 (cyclo-oxygenase-2) and, therefore, has anti-inflammatory, analgesic and antipyretic activities[1,2]. When administered in recommended dosage demonstrates low incidence of side effects and is better tolerated than other NSAIDs, such as diclofenac, ketoprofen, naproxen and piroxicam[1].

Nimesulide is a sulfonanilide derivative, with a melting point around 143 °C[2,3]. According to the literature, it is a weakly acidic (pK_a approximately to 6.5), attributed to the presence of a sulfonamide group[1,2]. It is practically insoluble in water (about 10 µg/mL) and soluble in methanol and ethanol at room temperature[4]. Based on Biopharmaceutics Classification System (BCS), nimesulide is considered a class 2 drug, characterized by low solubility and high permeability. Thus, its dissolution may represent a limiting step in drug absorption process[3].

According to one study reported in the literature, crystallization of nimesulide in different organic solvents affects some physicochemical properties such as melting point, solubility and dissolution profile, indicating the existence of

Eclética Química Journal, vol. 44, n. 3, 2019, 20-35
ISSN: 1678-4618
DOI: 10.26850/1678-4618eqj.v44.3.2019.p20-35

polymorphs[5]. Other studies describe the existence of two polymorphs of nimesulide: form I (usually used in the pharmaceutical industry) and form II[6,7].

Some studies discuss the characterization of nimesulide and demonstrated that DSC and X-ray diffraction techniques are promising in identifying polymorphs of nimesulide[7]. Additionally, the literature contains several studies using spectroscopy in the form of infrared complementary to other analytical techniques[7-10].

In terms of biopharmaceutical evaluation, a study obtained different values of intrinsic dissolution rate of nimesulide polymorphs I and II. However, the analysis of the graph in this study demonstrates that there was no linearity, affecting the results obtained in IDR[7]. Other studies using the intrinsic dissolution with this drug were not found, as well as studies using the wettability test. Allied to such trials, the powder dissolution has been used in biopharmaceutical evaluation[11,12], because there are some important factors that can impact on the assay results, for example, wettability, crystallinity, particle size and surface area[13].

The formulation studies evaluated the nimesulide tablets dissolution profile and found that drug release is not achieved even by testing the presence of surfactant at different concentrations in the dissolution medium[14,15].

Reducing the particle size of the drug to microparticles has been shown to significantly increase the dissolution and bioavailability of drugs. This is achieved by increasing the contact surface, which has a positive impact on the dissolution rate and possibly absorption[16]. One method to reduce particle size is by micronization[17] however, although there are advantages regarding the optimization of the dissolution of drugs with low solubility, micronizing should be carefully considered, because this can result in low density problems and inadequate flow. Accordingly, with respect to flowability, the literature reports a previous study evaluating the fluidity, in which it was demonstrated that nimesulide has no good flow properties[9].

The objective of this study was the characterization of nimesulide samples from different manufacturers and the development of immediate release tablets, in order to register a generic product. It was also tried to make some correlation between raw material characteristics and the final properties of the tablets in order to establish a different specification for quality control.

2. Materials and methods

2.1. Materials

Samples of nimesulide from three different manufacturers were coded as NM1 (sample non-micronized), NM2 and NM3 (micronized). The excipients microcrystalline cellulose 101 (Mingtai), lactose monohydrate 80 (DFE Pharma), sodium lauryl sulfate (Nuclear), docusate sodium (Shin-Etsu Chemical), sodium starch glycolate (Ecadil), low substituted hydroxypropyl cellulose (Shin-Etsu Chemical), polyvinylpyrrolidone K-30 (Boai Niki) and magnesium stearate (Magnesia), previously tested and approved according to the USP[18], were used. Standard sample of nimesulide was supplied by National Institute for Quality Control in Health, with purity of 99.80% and Nisulid®, Aché Laboratory, as the reference medicine.

2.2. Evaluation of the active pharmaceutical ingredient according to pharmacopoeia criteria

Samples NM1, NM2 and NM3, were analyzed according to the methodologies described in the Brazilian Pharmacopoeia[4]. The tests included identification, which used the method of infrared spectroscopy (spectrometer infrared model Nicolet 6700 FT-IR, Thermo Scientific), heavy metals, loss on drying, sulfated ash and dosing. This last one, followed the recommendations established in the method B of the Brazilian Pharmacopeia, which uses spectrophotometry absorption in the ultraviolet (LAMBDA 25, PerkinElmer) and the absorbance readings were performed at 392 nm.

2.3. Differential scanning calorimetry (DSC)

The DSC analysis was performed with a differential exploratory calorimeter instrument model 60, Shimadzu. The samples were weighed (about 3 mg) and encapsulated in aluminum crucibles with lid closed. The DSC curves were obtained under heating rates of 5, 10, 20 and 40 °C/min over a temperature from 25 to 200 °C, a flow rate of 50 mL min^{-1} of argon gas. Assays

Eclética Química Journal, vol. 44, n. 3, 2019, 20-35
ISSN: 1678-4618
DOI: 10.26850/1678-4618eqj.v44.3.2019.p20-35

were performed in triplicate. Different heating rates were used.

2.4. Fourier transform Infrared spectroscopy

The FTIR spectra were record using a Thermo Scientific, model Nicolet 6700 FT-IR, over a range from 4000 to 400 cm^{-1} at a resolution of 4 cm^{-1}. IR samples were analyzed directly without sample preparation.

2.5. X-Ray Powder Diffraction

The XRPD patterns of the samples were record on an X-ray D8 diffractometer (Bruker) equipped with Lynxeye XE detector and with Cu as tube anode (Kα radiation with λ = 1.5418 Å). The diffraction patterns were record under the following conditions: voltage 40 kV, 40 mA and fixed divergence slit using configuration of 2θ range from 4 to 50°, with a step size of 0.02° and a step time of 0.1 s. The identification of the crystal structure was performed using the database Cambridge Structural Database (CSD)[19] and calculated XRD pattern was prepared using the program Mercury 3.7[20].

2.6. Determination of particle size distribution using laser diffraction analysis

Particle size distribution was obtained by the laser diffraction method with a Malvern equipment, Model 2000E Mastersizer, using the liquid mode, a measurement range of 0.1-500 μm and obscuration between 17 and 23%. The suspension of 500 mg of nimesulide was prepared with an aqueous solution containing 0.5% polysorbate 80, in a total of around 30 mL. It was necessary to use ultrasound (USC 2800A, Unique) with speed 10.

2.7. Scanning Electron Microscopy (SEM)

To study the morphology of NM samples, SEM was performed on a Quanta 400 microscope (FEI), at a voltage 10 kV, using 500 and 16000x magnification. Small amounts of sample were adhered on a metal stub using double-sided adhesive carbon tape, which were then vacuum-coated (0.6 mbar) with a thin layer of gold in a BAL-TEC SCD 005 sputter coater at room temperature.

2.8. Wettability

The analysis was conducted with a tensiometer Krüss, DSA 100 at room temperature by sessile drop method. Approximately 300 mg were compressed in the form of discs using 800 psi for 1 min with the aid of a hydraulic press. The liquid drop (water saturated with nimesulide) was dispensed onto the surface of the sample and the images were captured immediately. The instrument calculated the contact angle by fitting mathematical expression to the shape of the drop.

2.9. Powder dissolution

Powder dissolution was performed with a dissolutor Distek, model 6100, and the conditions were as follows: 900 mL of potassium phosphate buffer solution adjusted to pH 7.4, with 2.0% polysorbate 80 (w/w) at 37 ± 0.5 °C and stirred with apparatus II (paddle) at 75 rpm rotating speed. Approximately 100.0 mg of nimesulide were added directly to the vessels and aliquots of 10 mL were collected after 5, 10, 15, 20, 30, 45, 60 and 90 min, without replacing the medium. Aliquots were filtered through 45 μm polytetrafluoroethylene filter, diluted and the absorbance measured in a spectrophotometer (LAMBDA 25, PerkinElmer) at a wavelength of 392 nm. The tests were performed in triplicate. A comparison of the dissolution profiles dispersion was made by calculating the difference factor (F1), the similarity factor (F2) and the dissolution efficiency (DE). The DE values were submitted to statistical analysis of variance (one-way ANOVA) followed by Tukey test and considered significant $p < 0.05$.

2.10. Determination of flowability

The evaluation of the flowability was carried out by the bulk and tapped density, Carr index, Hausner ratio, repose angle and flow through an orifice determination. The densities were determined according method I of USP[18], using the equipment Tap Density Tester (Nova Ética). The values were used to calculate the Carr's index and Hausner ratio. For the determination of repose angle and flow through an orifice was used Granulate GTB Tester Equipment (Erweka) with different diameter orifices and rotation speed to determine the optimal test conditions and

Eclética Química Journal, vol. 44, n. 3, 2019, 20-35
ISSN: 1678-4618
DOI: 10.26850/1678-4618eqj.v44.3.2019.p20-35

discriminate the flowability profiles of the samples.

2.11. Formulation design

The galenic batches were prepared in amounts about 600 to 800 g. The wet granulation was conducted with a high shear granulator capacity 4 L (TMG 1/6, Glatt), for the initial powder mixture and the wetting with the binder solution. After the granulation, the wet mass was passed through a mesh of 4 mm using the oscillating granulator (K-70, Lawes). The drying of the granulate was performed in a fluidized bed (midi Glatt, Glatt), at a temperature of 45 °C under a controlled flow. The end point was determined by drying the residual humidity using an infrared balance (IV2500, Gehaka) and was established a range between 2 and 3%. After drying, the granulate was normalized with a mesh of 1.5 mm in the oscillating granulator. Then, this granulate was transferred to a V-blender, capacity 2 L (66/10, Lawes), to perform the mixing of the excipients that were added in the extra granular phase. Finally, the compression was performed on a rotating compressor (2000 10PSC, Lawes), fitted with punches of 10 mm flat. The process control was carried out by checking the weight, hardness, friability and disintegration of the tablets. For such determinations was used the following equipments: semi-analytical balance, capacity 200 g (Sartorius), portable durometer (TBH100, Erweka), friability tester (TA10, Erweka) and disintegrator (301-1, Nova Ética).

2.12. Evaluation of galenic batches

The tablets were analyzed by the average weight, hardness, friability and disintegration, conducted as described in Brazilian Pharmacopoeia[4], and the comparative dissolution profile, was carried out with the Nisulid® reference drug.

2.13. Dosing

The analysis was performed according to the Brazilian Pharmacopoeia[4], which quantifies the nimesulide content in tablets by ultraviolet absorption spectrophotometry at a wavelength of 392 nm. The assay was performed in triplicate with the standard solution and the sample solution.

2.14. Dissolution profile

Initially, the dissolution profiles were performed using the conditions recommended by the Brazilian Pharmacopoeia[4], with the reference product and the galenic batches who presented the results of physical tests (hardness, disintegration and friability) most promising. The analytical conditions were: 900 mL of potassium phosphate buffer, pH 7.4, containing 2.0% (v/v) polysorbate 80 and stirred with paddle at a rotation speed of 75 rpm. Aliquots of 10 mL were removed after 5, 10, 15, 20, 30 and 45 min, without replacing the medium, maintaining sink conditions throughout the test. The amount of drug dissolved was determined by reading on a spectrophotometer (UV-1800, Shimadzu) in the ultraviolet region at a wavelength of 392 nm. Then, one of the galenic formulations, which showed the same type of dissolution to the reference product has been selected to perform additional dissolution profiles studies. For this, was used the dissolution medium potassium phosphate buffer, pH 7.4, containing polysorbate 80 in concentrations of 1.0% and 0.5%. The others analytical conditions were maintained. The dissolution profiles were compared using dissolution efficiency (DE) and their values were submitted to statistical analysis of variance (one-way ANOVA) followed by Tukey test and considered significant $p < 0.05$.

3. Results

3.1. Evaluation of the active pharmaceutical ingredient according to pharmacopoeia criteria

The results of heavy metals, loss on drying, sulfated ash and dosing match the specifications of the Brazilian Pharmacopoeia[4] and are presented in Table 1.

Eclética Química Journal, vol. 44, n. 3, 2019, 20-35
ISSN: 1678-4618
DOI: 10.26850/1678-4618eqj.v44.3.2019.p20-35

Table 1. Results of heavy metals, loss on drying, sulfated ash, dosing, contact angle of NM1, NM2 and NM3 samples.

	Sample		
	NM1	NM2	NM3
Heavy metals (ppm)	< 20 ppm	< 20 ppm	< 20 ppm
Loss on drying (%)	0.19	0.21	0.34
Sulfated ash (%)	0.04	0.03	0.03
Dosing (%)	99.5	99.2	99.6
Contact angle (°) (average ± SD)	80.7 ± 1.7	79.1 ± 3.0	78.8 ± 3.3

3.2. Differential scanning calorimetry (DSC)

The DSC curves obtained for NM1, NM2 and NM3 samples, measured at a heating rate of 5 °C/min showed a single sharp endothermic peak at approximately 149 °C in accordance with the melting point measurements (Figure 1). The same results were obtained in the DSC curves for NM1 sample under other conditions as 10, 20 and 40 °C min^{-1}. In addition, NM2 and NM3 showed identical results. For NM1, NM2 and NM3 samples, the baseline of DSC curves was similar and display that the thermal capacity was not changed by micronization process.

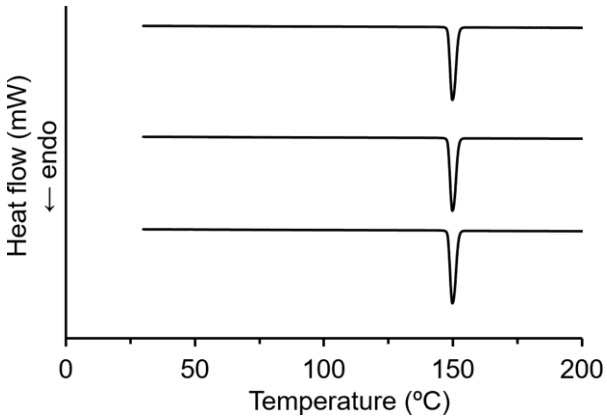

Figure 1. DSC curves from bottom to top NM1, NM2 and NM3 samples at a heating rate of 5 °C/min.

3.3. Infrared Spectroscopy

The FTIR spectra of all samples were equivalent (data not shown). The IR spectrum showed the ν_{NH} at 3278 cm^{-1}, a band at 1149 cm^{-1} assigned to the symmetric deformation of SO_2 group, ν_{NO2} stretching frequencies at 1330 cm^{-1} and 1588 cm^{-1} and a band at 1246 cm^{-1} assigned to the ν_{COC}. Except for the ν_{NH} and ν_{NO2} (at 1588 cm^{-1}), that presented weak intensity peaks, all the others functional groups of nimesulide demonstrated medium intensity peaks.

3.4. X-Ray Diffraction

The X-ray diffraction patterns of NM1, NM2 and NM3 samples (Figure 2) presented characteristic peaks at approximately 2θ = 17.07, 18.14, 19.35 and 21.60°. The samples comparison data clearly showed that the micronization process did not change the NM structure. The results were compared with the data of NM polymorphs I and II calculated from CSD and are also shown in Figure 2.

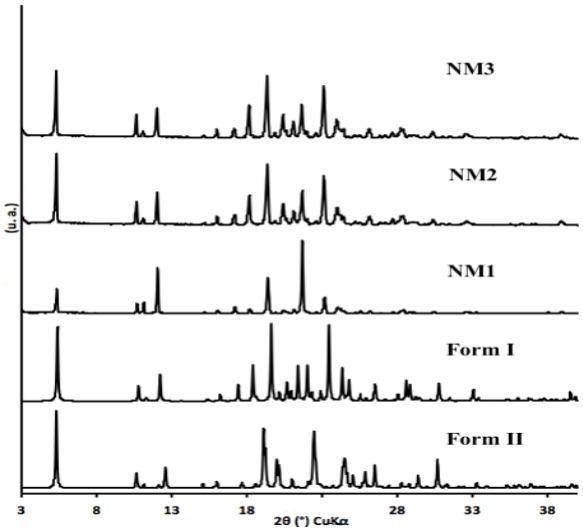

Figure 2. X-Ray diffraction patterns of the samples NM1, NM2 and NM3 and calculated patterns of the polymorphs I and II of nimesulide obtained from the CDCC (The Cambridge Crystallographic Data Centre).

Eclética Química Journal, vol. 44, n. 3, 2019, 20-35
ISSN: 1678-4618
DOI: 10.26850/1678-4618eqj.v44.3.2019.p20-35

3.5. Particle size distribution using laser diffraction

The average size of particles results, the values of particles smaller than 10% (d10), 50% (d50), and 90% (d90) and the results of dispersibility indices (span) was obtained with the samples from different manufacturers of nimesulide. The NM3 sample showed the smallest particle size (d10 = 1.28; d50 = 6.57 and d90 = 20.61), followed very closely by the NM2 sample (d10 = 2.09; d50 = 8.46 and d90 = 20.89) and, finally, the non-micronized sample (NM1) showed the largest particle size (d10 = 10.34; d50 = 33.85 and d90 = 76.52). Comparison of dispersibility indices indicate that NM3 sample has the greater nonuniformity of particle size distribution (DI = 2.94), followed by NM2 sample (DI = 2.22) and, finally, NM1 sample (DI = 1.96). The particle size distribution graphs are shown in Figure 3.

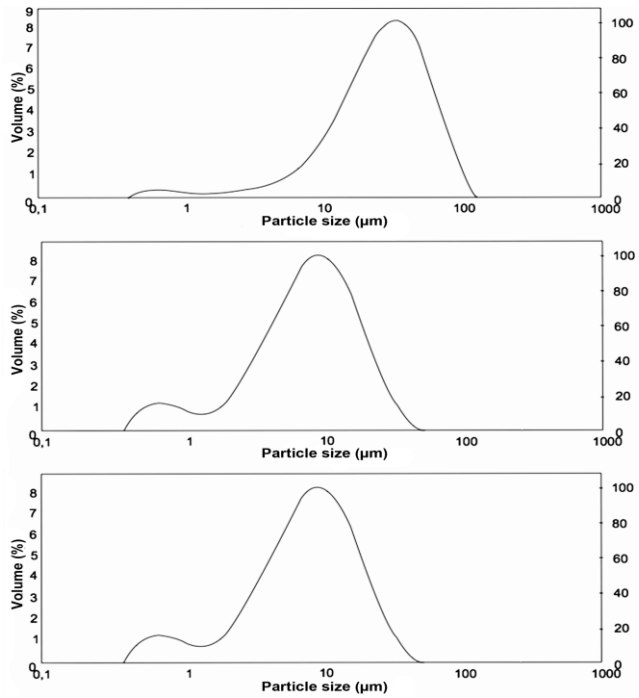

Figure 3. Particle size measurements obtained by LASER diffraction from bottom to top NM1, NM2 and NM3 samples.

3.6. Scanning electron microscopy (SEM)

The images of the samples under study, obtained by SEM at 500x magnification for NM1 and 16.000x for NM2 and NM3 samples, are shown in Figure 4. The NM1 sample presented the highest particle sizes between 25.2 and 103.5 µm, which was previously expected because is the IFA non-micronized, while the micronized NM2 and NM3 samples showed particles in the range of 364.8 nm to 3.5 µm (Figure 4 B, C). The micronization process led to the formation of aggregates.

3.7. Wettability

Table 1 presents the results for all samples, being observed that, using the method of the sessile drop and water as wetting agent, they were all near 80°.

3.8. Powder dissolution

Comparison of dissolution dispersion profiles of NM1, NM2 and NM3 samples is shown in Figure 5 and the values of F1, F2 and DE were established. The F1 and F2 values (15.26 and 46.23, respectively) confirm that the NM1 and NM3 samples showed the greatest differences between the profiles. The result of F1 for the micronized samples (NM2 and NM3) also showed a high value (12.36) and a considerably borderline result for the F2 parameter (50.55). Less expected, the F1 and F2 values that showed the greatest similarity was when the dissolution profiles of NM1 (non-micronized) and NM2 (micronized) were compared (3.33; 69.29). The DE values were statistically analyzed by ANOVA and significant differences were detected ($p < 0.05$). However, when using the Tukey test, it was found that there were no significant differences between the DE values of NM1 and NM2 profiles (DE = 71 ± 2 and 74 ± 5, respectively), while the significant differences were encountered between the profiles NM1 and NM3, NM2 and NM3 (DE = 83 ± 1).

Eclética Química Journal, vol. 44, n. 3, 2019, 20-35
ISSN: 1678-4618
DOI: 10.26850/1678-4618eqj.v44.3.2019.p20-35

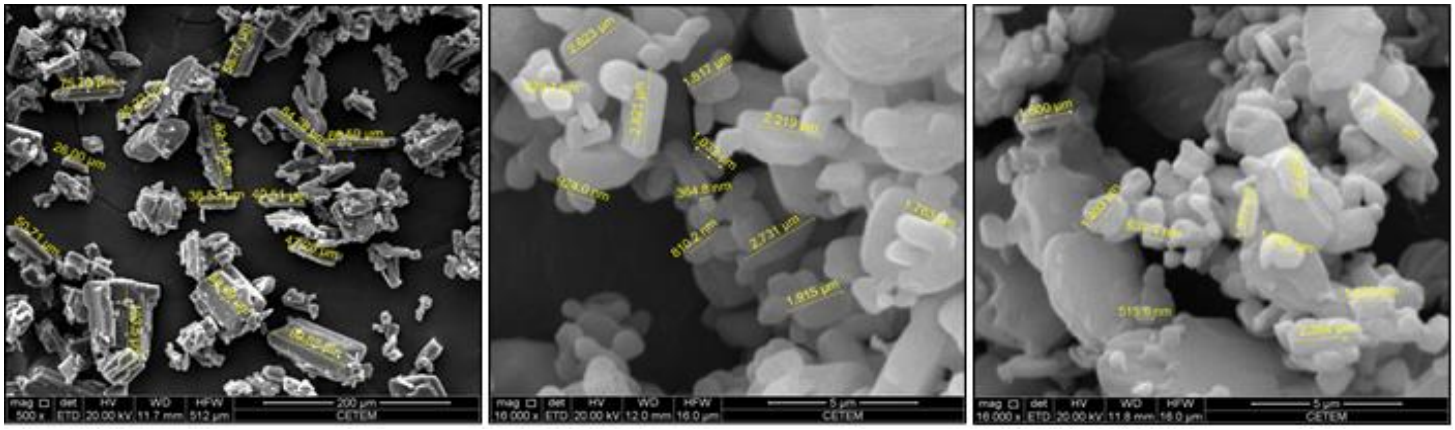

Figure 4. Scanning electron microscopy of the samples NM1, NM2 and NM3 from top to down, with measurements with increase of 500, 20Kv for NM1 and 16.000 X for NM2 and NM3.

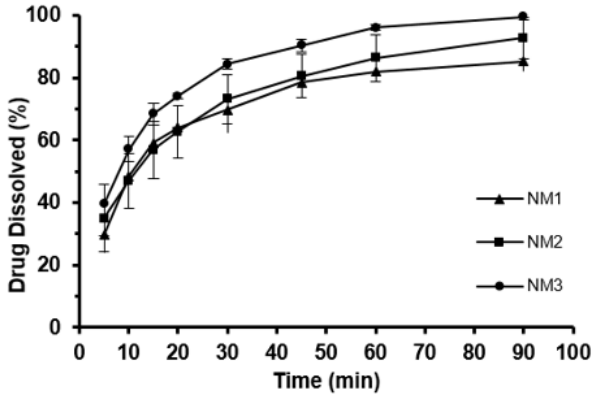

Figure 5. Powder dissolution profiles of NM1, NM2 and NM3 samples in 900 ml of potassium phosphate butter, pH 7.4, containing 2.0% polysorbate 80 (V/V), using paddle apparatus at 75 RPM.

3.9. Determination of flowability

3.9.1. Bulk and tapped density, compressibility index and Hausner ratio

The values obtained in bulk and tapped densities tests and the flow ratings of nimesulide samples found for the compressibility index and Hausner ratio were established according to the recommendations by USP[18] and are shown in Table 2. Densities obtained for the sample NM1, although slightly larger, still represent lower density values. The lower values for the densities of NM2 and NM3 samples are consistent with their smaller size particles.

Table 2. Data obtained from the DSC curves Tonset, Tpeak and enthalpy (ΔH) for the samples NM1, NM2 and NM3 in different heating rates.

Properties	**Sample**	**Heating rate (°C/min)**			
		5	10	20	40
T_{onset} ± SD (°C)	NM1	148.3 ± 0.3	148.5 ± 0.3	149.0 ± 0.6	150.8 ± 0.7
	NM2	147.9 ± 0.3	148.2 ± 0.4	148.8 ± 0.5	149.8 ± 0.4
	NM3	147.6 ± 0.2	147.8 ± 0.3	148.6 ± 0.4	149.8 ± 0.3
T_{peak} ± SD (°C)	NM1	149.8 ± 0.3	150.8 ± 0.3	152.5 ± 0.5	157.0 ± 0.6
	NM2	149.2 ± 0.3	150.1 ± 0.3	151.4 ± 0.5	153.5 ± 0.5
	NM3	149.1 ± 0.2	149.4 ± 0.3	151.2 ± 0.4	154.0 ± 0.3
ΔH ± SD (J/g)	NM1	121.6 ± 0.3	111.8 ± 0.4	112.2 ± 0.6	120.1 ± 0.7
	NM2	111.8 ± 0.4	110.7 ± 0.8	111.7 ± 0.5	116.7 ± 0.6
	NM3	109.7 ± 0.3	109.7 ± 0.4	107.6 ± 0.5	113.0 ± 0.4

Eclética Química Journal, vol. 44, n. 3, 2019, 20-35
ISSN: 1678-4618
DOI: 10.26850/1678-4618eqj.v44.3.2019.p20-35

3.9.2. Determination of repose angle and flow through orifice

The repose angle could not be determined due to the poor flowability of the samples. The graphs obtained by the flow through orifice are shown in Figure 6 and the results are featured in Table 2.

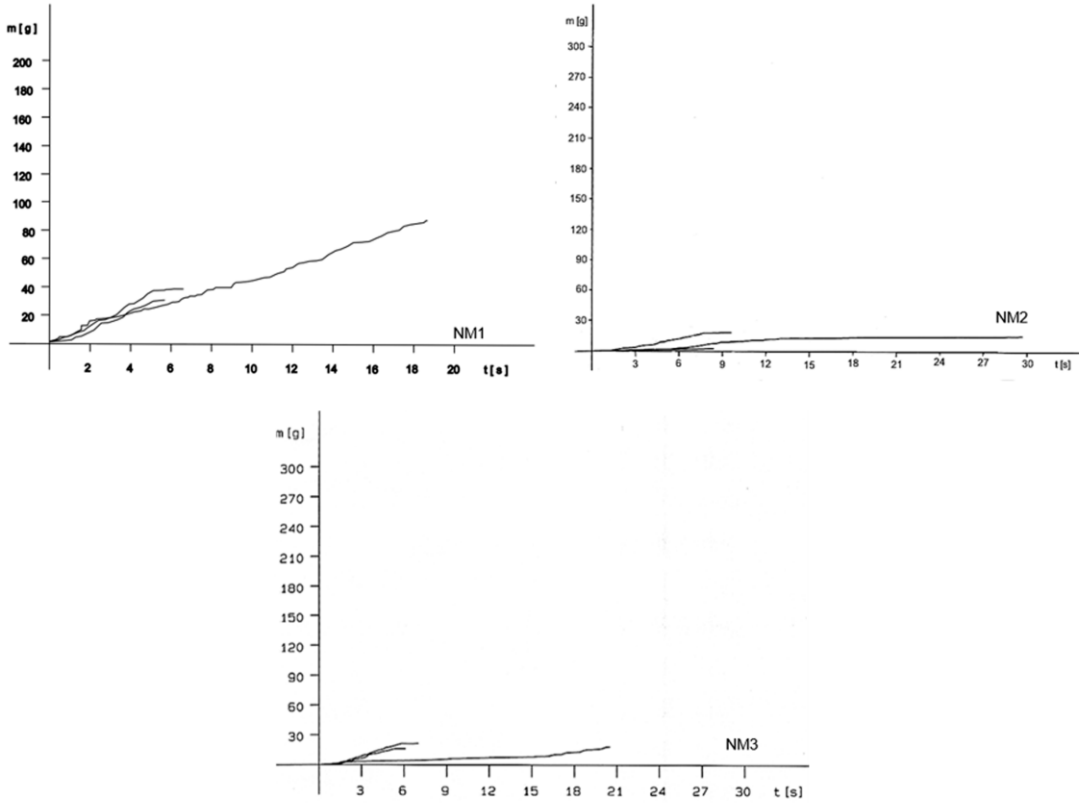

Figure 6. Graphs oof low through orifice of NM1, NM2 and NM3 samples.

3.10. Development and evaluation of nimesulide tablets obtained in galenic batches

The design of the galenic formulations batches was conducted with the excipients commonly used in the pharmaceutical industry, besides the excipients present in the reference product formulation. The excipients lactose monohydrate, microcrystalline cellulose, hydroxypropylcellulose, sodium starch glycollate, docusate sodium, hydrogenated vegetable oil and magnesium stearate are present in the formulation of Nisulid®. The galenic batches used the same excipients except by the hydrogenated vegetable oil and formulations with polyvinylpyrrolidone K-30 and pregelatinized starch as a binder in place of hydroxypropylcellulose, and sodium lauryl sulfate, as the surfactant, instead of sodium docusate were also tested. The galenic batches (Table 3) used only the micronized samples, NM2 and NM3, due to the better results in powder dissolution than the API non-micronized (Figure 5).

3.10.1. Physical parameters of the tablets and dosing

The results of weight, hardness, friability and dosing were all satisfactory. The disintegration test showed some unsatisfactory results, represented by L5 batch with a relatively high disintegration time (L5 = 9’ 30”), especially when compared to the reference product, (1’ 15”) besides L6 that was out of specification (L6 = greater than 30’). Therefore, it was decided not to perform the dissolution profiles of these batches.

Eclética Química Journal, vol. 44, n. 3, 2019, 20-35
ISSN: 1678-4618
DOI: 10.26850/1678-4618eqj.v44.3.2019.p20-35

Table 3. Flowability measurements of NM1, NM2 and NM3 samples (n=3).

Properties	Sample		
	NM1	NM2	NM3
Bulk density ± SD (g/mL)	0.45 ± 0.01	0.20 ± 0.02	0.19 ± 0.02
Tapped density ± SD (g/mL)	0.69 ± 0.01	0.28 ± 0.02	0.26 ± 0.02
Compressibility index (rating)	34.78 (very poor)	26.53 (poor)	27.69 (poor)
Hausner ratio (rating)	1.53 (very poor)	1.36 (poor)	1.38 (poor)
Repose angle	ND	ND	ND
Flow through orifice (s/100 g* – RSD %)	18.8 (17.0-21.3) ± 11.78%	61.0 (32.7-112.0) ± 72.69%	189.6 (52.7-323.1) ± 71.34%

ND not determined

* The results expressed are the average obtained regarding the determination in triplicate samples. The values in brackets refer to the range found in the analysis, with minimum and maximum values.

3.10.2. Dissolution profile

3.10.2.1. Dissolution profiles conducted according to the criteria of the Brazilian Pharmacopoeia

Initially, the dissolution profiles were performed with the galenic batches L1, L2, L3, L4, L7 and the reference product using the conditions recommended by the Brazilian Pharmacopoeia[4] and are shown in Figure 7. In these tests, the reference product showed values greater than 85% of dissolution in 15 minutes, while only L2 and L3 batches showed a very fast dissolution profile, same behavior of the reference product. The statistical analysis has shown that DE values of L2 and L3 dissolution profiles (DE = 84.95 and 84.02, respectively) are not significantly different ($p > 0.05$). However, it was decided to select the L2 batch for the evaluation of the influence of the surfactant in the medium dissolution recommended by the Brazilian Pharmacopoeia (polysorbate 80 2.0%) in different concentrations.

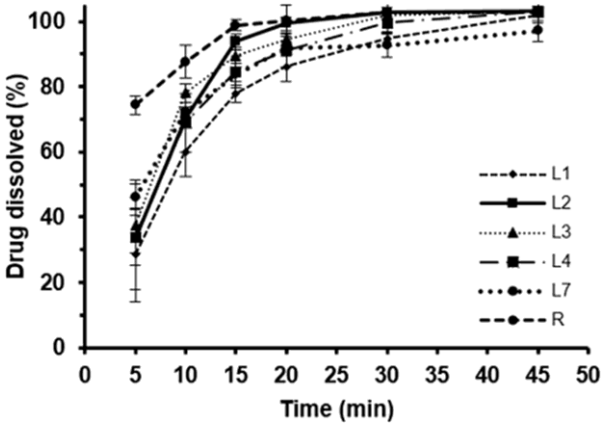

Figure 7. Overlap of L1, L2, L3, L4, L7 dissolution profiles and the reference product (R) using the pharmacopoeic parameters (BF 5, 2010).

3.10.2.2. Dissolution profile in potassium phosphate buffer, pH 7.4, containing different concentrations of polysorbate 80

The curves of dissolution profiles containing different concentrations of polysorbate 80 obtained with the tablets of L2 batch and Nisulid® is illustrated in Figure 8. The presented results show a reduction in drug release as the concentration of polysorbate 80 has been reduced. In all assessed surfactant concentrations, the test product and the reference product remained values above 85% over 15 minutes maintaining the very rapid dissolution classification and making it unnecessary the determination of F2. The dissolution efficiency was calculated to compare dissolution profiles. There was a reduction in DE when the concentration of the surfactant was gradually removed from the dissolution medium.

Eclética Química Journal, vol. 44, n. 3, 2019, 20-35
ISSN: 1678-4618
DOI: 10.26850/1678-4618eqj.v44.3.2019.p20-35

This occurred for both the L2 batch (DE = 84.95; 82.21 and 80. 41, respectively with 2.0% polysorbate, 1.0% and 0.5%) as for the reference product (DE = 90. 83; 90. 53 and 87.05, in the same conditions). Statistical analysis by ANOVA revealed that the dissolution profiles are statistically different ($p < 0.05$) and the Tukey's test identified that in each condition evaluated (polysorbate 80 2.0%, 1.0% and 0.5%), the dissolution profile of L2 batch was statistically different from the reference product. The sodium lauryl sulfate present in the formulation would enhance the percentage of this surfactant in the dissolution medium at a maximum of 0,1%.

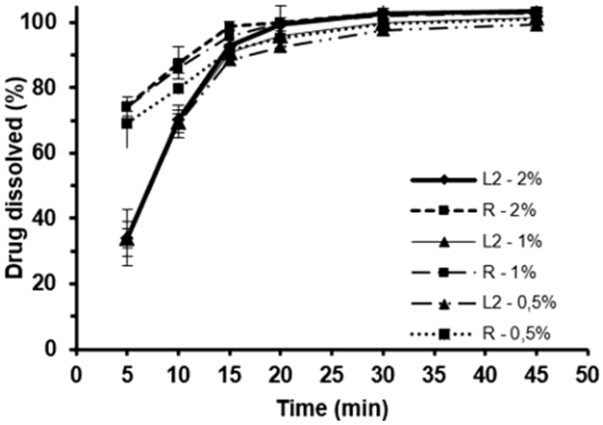

Figure 8. Overlap of dissolution profiles of L2 batch and the reference product (R) in potassium phosphate buffer, pH 7.4, containing different concetrations of poysorbate 80 (2.0%, 1.0% and 0.5%).

4. Discussion

The pharmacopoeia tests related to the heavy metals determination, loss on drying, sulfated ash and dosing, performed with NM1, NM2 and NM3 samples were approved by the specifications of the Brazilian Pharmacopoeia 2010 (Table 1). The differences between the dosing of galenic batches (approximately 95%) and the reference product (100.16%) are assigned to the manual transfers of high shear for oscillating granulator, and hence to the fluidized bed, procedures that, in industrial scale, occur in an automatic way.

The DSC curves of NM1, NM2 and NM3 showed a single endothermic event close to 149 °C (Figure 1). The evaluation of the T_{onset}, T_{peak} and ΔH values obtained in different heating rate showed slightly lower values to the micronized samples (NM2 and NM3, around 110-120 J/g). This phenomenon is widely described in the literature regarding DSC[21].

Previous studies reported the melting point of NM form I over the range of 148.9 to 151.0 °C and enthalpy (ΔH) of 102.97 J/g and 127.4 J g^{-1} [9,22,23]. These studies used different analysis conditions of each other and from this work, especially regarding the purge gas, heating rate and the types of crucible. Thus, although the results are very close to the literature data, such differences limit a more reliable correlation.

A study reported that NM form I is the most thermodynamically stable and has a transition temperature over the range of 144-147 °C (ΔH = 107.63 J/g)[7]. Otherwise, polymorph II has an endotermic event at 140 °C and suffers a transition to polymorph I (melting point at 144 °C and ΔH = 105.97 J/g)[6,7]. The DSC curves (Figure 1) of all NM samples showed similar thermal behavior to that of polymorph I.

There are not major differences between the FTIR spectra of NM1, NM2 and NM3 samples that could be used to distinguish among polymorph I and II. Only the characteristic bands of nimesulide were identified, so although this technique is often used to discriminate between polymorphs in this case it was inconclusive[7,10].

The X-ray powder diffraction is the standard method to distinguish between different polymorphs. In the case of nimesulide, there are noticeable differences in the peak position of form I (2θ = 17.15, 18.13, 19.34 and 21.66°) and form II (2θ = 18.91, 22.15 and 26.14°)[6]. In addition, diffraction patterns in the CSD revealed peaks at 2θ = 17.38, 18.38, 19.62 and 22.00° for form I and 2θ = 19.10, 22.44 and 25.84° for form II. The XRPD patterns of nimesulide samples analyzed correspond to the form I, although the NM1 (non-micronized sample) have shown differences in peak intensities (Figure 2). Besides, the literature mentions the occurrence of preferred orientation in X-ray diffraction of nimesulide samples, resulting in peaks of different intensities, but always in the same position, which characterizes the same crystalline arrangement.

A review of the particle size distribution graphs (Figure 3) allows to observe the presence of more than one population of particle sizes, primarily evidenced in micronized samples (NM2 and NM3) below 1 µM, which represents a bimodal distribution curve. Often, micronization causes difficulties in a good dispersion, assigned to cohesive interparticle properties and electrostatic forces provided by the particles that are subjected to this process. The sample NM1

Eclética Química Journal, vol. 44, n. 3, 2019, 20-35
ISSN: 1678-4618
DOI: 10.26850/1678-4618eqj.v44.3.2019.p20-35

non-micronized has a particle size population below 5 µm, but less significant compared with the population of particle sizes below 1 µM detected in micronized samples.

During the development of a solid dosage formulation, the knowledge of the size and distribution of particle size can be used to guide the selection of a process by direct compression or wet granulation. The results obtained from laser diffraction were used together with the results of the flowability evaluation in order to complement the choice of manufacturing process of nimesulide tablets.

The data obtained by SEM confirmed the results of particle size distribution by laser diffraction, in which NM1 sample also showed much higher particle sizes compared to the NM2 and NM3 samples (Figure 4). Additionally, the presence of a population of particles with sizes close to 1 µM in NM2 and NM3 samples and 5 µm in NM1 sample, observed in the particle size distribution by laser diffraction, were also observed in the SEM. The image of NM1, although demonstrating a certain variability in their morphology, shows elongated particles. The images of NM2 and NM3 micronized samples showed greatest similarity regarding the particle sizes and can also be observed the formation of aggregates (Figure 4B and C).

The results of the wettability test were all close to 80° (Table 1) and, in accordance with literature, the values close to 90° predict a poor wettability[24]. Although the literature does not present studies applying wettability test with nimesulide, some works with other drugs were conducted, in which the results of the contact angles were correlated with water solubility[25,26,27].

When the aim is the development of a tablet formulation, the low solubility of the drug is an aspect that reflects negatively on its bioavailability. The powder dissolution tests served as an important tool to complement the biopharmaceutical evaluation of nimesulide samples. The literature revealed some studies using powder dissolution tests with nimesulide samples and the results have a certain proximity to that found in this study[22,28]. However, the studies referenced used different analytical conditions, especially with regard to the dissolution medium and the rotation apparatus, which compromise the correlation results.

Differently from the laser diffraction results, which showed a very small difference between NM2 and NM3, in the powder dissolution, these samples did not demonstrate similar behavior, which can be verified by NM3 superior performance relatively to NM2 (Figure 5). The non-micronized sample (NM1) presented larger particle sizes when compared to micronized samples and, however, in the powder dissolution, NM1 showed values near NM2. Thus, other factors that impact the powder dissolution results should be considered as the presence of electrostatic charge and the trend to agglomerate, which could undertake the performance of NM2 sample.

It was also not possible to establish a direct relationship of the results obtained in the wettability with the results of powder dissolution because, as mentioned above, the values of contact angles provided by the samples of nimesulide were very close (Table 1).

The evaluation of flowability brought together the results of different methods in order to make more complete the understanding of the flow properties of the samples under study. The densities obtained for the NM1 are low (Table 2), showed values slightly higher the other samples. The literature shows results of bulk and tapped density for nimesulide samples near to that of the non-micronized NM1. However, for the tapped density, the referenced study used a different method, making questionable the correlation to the results presented here[13]. The lower values for the densities of NM2 and NM3 can be explained by the effect of the micronization process, which results in powders having greater adhesion between the particles and therefore a greater tendency to agglomerate. The result is a poor flow material with low apparent density.

The determination of the compressibility index and Hausner ratio showed that all samples did not have good flow properties (Table 2). Considering that the higher values for compressibility index and Hausner ratio indicate stronger interparticle interactions and undesirable flow characteristics[29], it would be expected that micronized samples, NM2 and NM3, would demonstrate the worst results of flow. However, they presented better flowability rating than that exhibited by the sample NM1 (non-micronized).

One possible explanation for the discrepancies between the results found in the various flowability assessments lies in the qualitative scale of classification for flow properties adopted by official compendia, for example, the US

Eclética Química Journal, vol. 44, n. 3, 2019, 20-35
ISSN: 1678-4618
DOI: 10.26850/1678-4618eqj.v44.3.2019.p20-35

Pharmacopeia. Thus, the CI and HR parameters have low discriminatory power, especially for the poor flow samples.

The repose angle and the flow through orifice tests were carried out in the same equipment. The tests with NM1, NM2 and NM3 samples were conducted using the following funnel openings 10, 15 and 25 mm. However, no flow was detectable. Then there was used the opening of 15 mm and tested four (4) speeds available on the machine (1, 2, 3 and 4). The NM1 sample showed flowability with speed 1 (one), but for the NM2 and NM3 samples, it was necessary to use the speed 4, maximum permitted by the equipment. The different experimental conditions undertake, somehow, the discussion of results. Still, it is possible establish some considerations concerning the flow properties of the samples under study.

The results confirmed the estimation of poor flow for this API, previously provided by other tests. Plus, it is also possible verify that no reproducibility was observed in the tests performed in triplicate. The NM1, non-micronized, revealed superior flow properties compared to the other samples. It is also possible assign a worse flow for NM3 sample, which also showed less uniform behavior (Figure 6).

In general, all samples showed erratic flow behavior, which indicates that an unstable formation and destruction process of the arc dominates the flow process. This process is also evidenced by the standard in “steps” where the powder flow rate accelerates periodically, probably due to the destruction of the formed ar.

It is known that the micronization process promotes a tendency to increased electrostatic charge. Thus, NM2 and NM3 samples have two important properties that contribute to a poor flow: low-density particles and, supposedly, high electrostatic charge. Unfortunately, for this work, it was not possible to assess electrostatic density.

The results obtained in flow assessment tests allow identify a discrepancy between the determinations of the CI and HR and flow through orifice. The flow through orifice provided more realistic results, demonstrating, numerically, the characteristic of poor flow for nimesulide. As mentioned above, HR and CI values may not be discriminatory and may cause unreal results flow to powders that are particularly characterized by poor flow. Furthermore, the samples NM1, NM2 and NM3 have particle sizes that are considered small (< 80 µM) besides low density values, which are factors related to the high cohesion of its particles. In this way, it is understandable that the flow evaluation methods may have discordant results.

Based on the results presented in flowability assessments, particle size distribution and SEM and considering the aim of the development of a solid dosage formulation, the direct compression process becomes less suitable than the wet granulation, due to the high possibility of problems related to the flow in the hopper and inadequate die filling that promotes, consequently, nonuniformity of mass and content.

The average weight values found for galenic batches are close to the average weight displayed for the reference product (about 400 mg) and the results were all satisfactory. The tablet hardness results obtained with the galenic batches showed correlation with those of friability, in which the L2, L3, L5, L6 and L7 batches showed the lowest hardness values (close to 5.0 kgf) and the higher friability values (near 0.42%) and the tablets obtained with the L1 and L4 galenic batches demonstrated higher strength, both to rupture (hardness assay about 7.0 kgf) and abrasion (friability percentage about 0.35%).

L2 and L3 batches have the same formulation and the same process by only changing the manufacturer of API (Table 3). The differences in results of particle size and hardness were not significant, preventing a direct correlation between these tests.

The L4 batch has the same qualitative and quantitative excipients that can influence the compressibility from the L2 and L3 batches but showed higher hardness (mean = 7.1 kgf). The difference was in the granulation process (Table 3) including a higher time to addition the granulating solution and a longer mixture for the L4 batch. Possibly, these process variations allow adequate wetting of the powders, resulting in stronger granules and, consequently, in longer disintegration time and slower dissolution compared to the values shown by L2 and L3 batches.

Regarding disintegration test, L1 batch has the same qualitative composition of L2 and L3, but the surfactant (sodium lauryl sulfate) was used in different ways. L1 showed the highest values in hardness assay (7.5 kgf). These differences had a negative impact on the disintegration of the tablets obtained with this batch (L1 = 6’ 40”), which had twice the disintegration time of L2 and L3 batches

Eclética Química Journal, vol. 44, n. 3, 2019, 20-35
ISSN: 1678-4618
DOI: 10.26850/1678-4618eqj.v44.3.2019.p20-35

(L2 = 3’ 18” and L3 = 3’ 10”). The L4 batch used another surfactant (sodium docusate) and its disintegration time (4’ 10”) was higher than the L2 and L3 batches. L5 and L6 formulations are closest qualitatively of the reference product, but showed more extensive disintegration times and L6, in this assay, was disapproved (L5 = 9’ 30” and L6 = greater than 30’). Obviously, this cannot attribute similarity or difference by not being aware of the percentages of each agent in the reference product formulation. The L7 galenic batch used different binder and surfactant and had the shortest disintegration time (1’ 23”). Regarding Nisulid®, the tablet format is convex which facilitates the maintenance of abrasion resistance, observed by the low value friability (0.27%), although its hardness is lower (4.9 kgf) as compared to galenic batch. The disintegration time of the reference product was 1’ 15”.

Accordingly, it can be concluded that the step in which the surfactant is added to the formulation, as well as tablet hardness, directly alter the disintegration time and, therefore, can be used as auxiliary tools to discriminate between nimesulide formulations.

In the dosing assay, all galenic batches showed results close to 95% of the labeled value, and for Nisulid® tablets there was obtained 100.2%. All results meet the specification preconized in the Brazilian Pharmacopoeia.

The dissolution profiles achieved in pharmacopoeia conditions demonstrated that the formulations of the L2 and L3 batches and the reference product exhibited very rapid dissolution with results of the amount of dissolved drug above 85% in 15 minutes and thus the value of F2 loses its discriminative relevance.

Whereas L2 and L3 batches are formulations that differ only in the API manufacturer, it is interesting correlate the results obtained in the dissolution profile and the data obtained in API characterization, particularly in particle size, wettability and powder dissolution assessments. The results of particle size analysis by laser diffraction and wettability were quite close. However, in the powder dissolution, NM3 showed dissolution of approximately 10% higher than NM2 and further such profiles showed statistically significant differences ($p < 0.05$). Although NM3 biopharmaceutical properties were higher than observed with NM2, the L2 and L3 formulated product showed near dissolution results and statistical analysis of ED values showed similarity between these profiles ($p > 0.05$).

The dissolution efficiency values were calculated and L2 batch had the highest result (DE = 84.95), although quite near the value presented by L3 (DE = 84.02). L4 and L7 shown next values (L4 = 80.92 and L7 = 79.67) and the L1 batch showed the lowest DE value (76.61). The DE values were subjected to statistical analysis by ANOVA and Tukey test, and it was found that all galenic batches formulations and Nisulid® differ significantly ($p < 0.05$) and the L2 and L3 batches do not present significant differences between the DE values ($p > 0.05$). The L4 batch showed a dissolution profile similar to those of L2 and L3, but with lower dissolution mean values and, particularly at 15 minutes, there was not reached 85% (although it was close), which results in the classification as a rapid dissolving formulation, distinct from that presented by Nisulid® and by the L2 and L3 batches. As occurred with L4, L7 not reached 85% drug release within 15 minutes, despite having very close behavior (Figure 7) and it is also classified as a rapid dissolving formulation.

An interesting feature of the L7 dissolution profile lies in the result obtained in the first sampling time, which was superior in almost 10% when compared with the result obtained with L3. One possible explanation is the dual nature of the pregelatinized starch, that acts not only as a binder but also as a disintegrate, which may be maximizing the release of the API in this initial time. The result of the disintegration assay (83 s) confirms this hypothesis, considering the smallest time shown.

Although the statistical analysis has shown that DE values of L2, L3 and L4 batches are not significantly different ($p > 0.05$), it was decided to select the L2 batch for complementary tests. Even if the L2 has showed the greatest dissolution of values, there is a considerable difference between L2 and the reference product in the first sampling times ($t = 5$ min and $t = 10$ min).

In terms of bioequivalence, the literature reports that nimesulide has rapid oral absorption[2]. A Brazilian study evaluated the bioequivalence of nimesulide tablets and Nisulid® and there were found for C_{max} values equivalent to 5.30 and 4.52 ng mL^{-1} and T_{max} of 2.23 and 3.32 h, respectively, for the reference and test products[30].

Analyzing such data from the literature and based on the dissolution assessments designed to

Eclética Química Journal, vol. 44, n. 3, 2019, 20-35
ISSN: 1678-4618
DOI: 10.26850/1678-4618eqj.v44.3.2019.p20-35

simulate physiological conditions and provided tools for the *in vitro* evaluation of bioavailability, the evaluation of C_{max} and T_{max} would not represent bioequivalence problems. This is because, after 45 min (lower time to reach C_{max} than those presented by the literature) L2 batch and the reference product already reach the same percentage of dissolution; so, it is expected the same release between the drug (test and reference) *in vivo* assays.

The AUC parameter requires a more careful analysis. Another study, mentioned a nimesulide bioequivalence study that showed disapproved results, having been previously approved in the pharmaceutical equivalence, which reinforces the alert for the interpretation of the results of this drug dissolution profiles[31]. Whereas nimesulide is a class II drug in the BCS, which the dissolution is the limiting step for the absorption, it becomes mandatory a careful design of the dissolution test.

Thus, even if the medium is preconized by the Brazilian Pharmacopoeia containing 2.0% polysorbate 80[4], it was considered important evaluate the behavior of the L2 batch using the same potassium phosphate buffer established for Brazilian Pharmacopoeia but containing different concentrations of surfactant.

The presented results show a reduction in drug release amounts as the concentration of polysorbate 80 has been reduced. Still, in all assessed surfactant concentrations, the test and the reference product values remained above 85% over 15 minutes, maintaining the very rapid dissolution classification and making it unnecessary the F2 calculation. However, the dissolution efficiency was calculated as a tool to compare dissolution profiles. Again, there was observed a reduction of the obtained values of DE as the concentration of the surfactant was gradually reduced in the dissolution medium. This occurred for both the L2 batch as for the reference product. Statistical analysis by ANOVA revealed that the dissolution profiles are statistically different ($p < 0.05$) and Tukey's test identified that in each condition evaluated (2.0%, 1.0% and 0.5% polysorbate 80), the dissolution profile of L2 batch is statistically different from the reference product.

The literature reports a study evaluating the dissolution profile of nimesulide tablets in a medium of phosphate buffer pH 7.4 containing different concentrations of polysorbate 80. The highest release value was in the presence of 2.5% surfactant, obtaining around 90% of dissolution in 60 min[21]. Another study evaluating the dissolution of commercial nimesulide tablets in sodium phosphate buffer pH 7.4 supplemented with 1.0% polysorbate 80 did not obtain values above 90% in 60 min[15].

Since both studies do not provide information about the composition of the test product, outcome differences found comparing with those showed here can be attributed to probable differences in formulations, given that the excipients can act in direct mode in the dissolution process. In addition to the important contribution of excipients in the rate and extent of dissolution, aspects such as, for example, the API particle size are striking features in the dissolution of solid dosage forms. These physicochemical properties were not available in the referenced work, limiting further discussion.

The *in vitro* dissolution tests are used in quality control of medicines and the development of new formulations. Depending on the drug class, such as nimesulide (Class II in the BCS), the results of a dissolution study can be closely related with in vivo performance. For these drugs, difficulties in selecting the dissolution medium are constantly found, which must reproduce the physiological conditions to ensure an *in vitro-in vivo* correlation and to discriminate different formulations[28].

5. Conclusions

Differential scanning calorimetry and X-ray diffraction showed that all samples tested (NM1, NM2 and NM3) presented polymorph I. The characterization of particle size showed good correlation with the density results and flow through orifice in which the micronized samples showed worse flow behavior when compared with the non-micronized sample. The scanning electron microscopy confirmed the results of size and particle size distribution carried out by laser diffraction.

Although the wettability results were very close, the powder dissolution identified small differences between the samples, demonstrating that the dissolution of the NM3 sample (micronized) was superior to the others. The micronized samples exhibited higher IDR than the non-micronized one (NM1) and, in this case, surface properties such as roughness and microstructural factors may be involved.

Eclética Química Journal, vol. 44, n. 3, 2019, 20-35
ISSN: 1678-4618
DOI: 10.26850/1678-4618eqj.v44.3.2019.p20-35

Although the results have shown a reduction in drug release as the surfactant concentration has been reduced in the dissolution medium of both products (test and reference), the classification as a very rapid dissolution formulation was maintained. Batch L2 was selected for further work toward product registration.

6. References

[1] Rainsford, K. D., Current status of the therapeutic uses and actions of the preferential cyclo-oxygenase-2 NSAID, nimesulide, Inflammopharmacology 14 (3-4) (2006) 120-37. https://doi.org/10.1007/s10787-006-1505-9.

[2] Singla, A. K., Chawla, M., Singh, A., Review Nimesulide: some pharmaceutical and pharmacological aspects-an update, J. Pharm. Pharmacol. 52 (5) (2000) 467-486. https://doi.org/10.1211/0022357001774255.

[3] Mircioiu, I., Anuta, V., Miron, D., Cojocaru, V., Orbesteanu, A. M., Mircioiu, C., *In vitro* dissolution of poorly soluble drugs in the presence of surface active agents - *in vivo* pharmacokinetics correlations. II. Nimesulide, Farmacia 61 (1) (2013) 88-102. http://www.revistafarmacia.ro/201301/issue12013art09.html.

[4] Farmacopeia Brasileira, 5th ed. Brasília: Agência Nacional de Vigilância Sanitária; 2010.

[5] Di Martino, P., Censi, R., Barthelemy, C., Gobetto, R., Joiris, E., Masic, A., Odou, P., Martelli, S., Characterization and compaction behaviour of nimesulide crystal forms, Int. J. Pharm. 342 (1-2) (2007) 137-44. https://doi.org/10.1016/j.ijpharm.2007.05.009.

[6] Bergese, P., Bontempi, E., Colombo, I., Gervasoni, D., Depero, L. E., Microstructural investigation of nimesulide-crospovidone composites by X-ray diffraction and thermal analysis, Compos. Sci. Technol. 63 (8) (2003) 1197-1201. https://doi.org/10.1016/S0266-3538(03)00078-2.

[7] Sanphui, P., Sarma, B., Nangia, A., Phase transformation in conformational polymorphs of nimesulide, J. Pharm. Sci. 100 (6) (2011) 2287-2299. https://doi.org/10.1002/jps.22464.

[8] Abdelkader, H., Abdallah, O. Y., Salem, H. S., Comparison of the effect of tromethamine and polyvinylpyrrolidone on dissolution properties and analgesic effect of nimesulide, AAPS PharmSciTech 8 (3) (2007) E110–E117. https://doi.org/10.1208/pt0803065.

[9] Dantu, A. S., Durai, R. V., Hari, B. N. V., Effect of impact and attrition milling on nimesulide for solubility enhancement, Int. J. App. Pharm. 5 (2) (2003) 1-7.

[10] Paiva, R. E. F., Abbehausen, C., Gomes, A. F., Gozzo, F. C., Lustri, W. R., Formiga, A. L. B., Corbi, P. P., Synthesis, spectroscopic characterization, DFT studies and antibacterial assays of a novel silver(I) complex with the anti-inflammatory nimesulide, Polyhedron 36 (1) (2012) 112-119. https://doi.org/10.1016/j.poly.2012.02.002.

[11] Agrawal, S., Ashokraj, Y., Bharatam, P. V., Pillai, O., Panchagnula, R., Solid-state characterization of rifampicin samples and its biopharmaceutic relevance, Eur. J. Pharm. Sci. 22 (2-3) (2004) 127-144. https://doi.org/10.1016/j.ejps.2004.02.011.

[12] Honorio, T. S., Pinto, E. C., Rocha, H. V., Esteves, V. S., dos Santos, T. C., Castro, H. C., Rodrigues, C. R., de Sousa, V. P., Cabral, L. M., *In vitro–in vivo* correlation of efavirenz tablets using GastroPlus®, AAPS PharmSciTech. 14 (3) (2014) 1244–1254. https://doi.org/10.1208/s12249-013-0016-4.

[13] Debnah, S., Suryanarayanan, R., Influence of processing-induced phase transformations on the dissolution of theophylline tablets, AAPS PharmSciTech. 5 (1) (2004) 1-11. https://doi.org/10.1208/pt050108.

[14] Purcaru, S. O., Ionescu, M., Raneti, C., Anuta, V., Mircioiu, I., Belu, I., Study of nimesulide release from solid pharmaceutical formulations in tween 80 solutions, Curr. Health Sci. J. 36 (1) (2010) 42-49. https://www.ncbi.nlm.nih.gov/pmc/articles/PMC3945268/.

[15] Ruella, A. L. M., Araújo, M. B., Pereira, G., Desenvolvimento de um teste de dissolução para comprimidos de nimesulida em meio que assegure condições sink, Lat. Am. J. Pharm. 28 (5) (2009) 661-667. http://www.latamjpharm.org/trabajos/28/5/LAJOP_28_5_1_3_5K6E9AQ727.pdf.

[16] Hetal, T., Bindesh, P., Sneha, T., A review on techniques for oral bioavailability enhancement of drugs, Int. J. Pharm. Sci. Rev. Res. 4 (3) (2010) 203-223. https://pdfs.semanticscholar.org/0dd6/cc180bdabeab5bc627dcbbff2567735f494f.pdf.

[17] Joshi, J. T., A review on micronization techniques, J. Pharm. Sci. Technol. 3 (7) (2011) 651-681. http://www.onlinepharmacytech.info/docs/vol3issue8/JPST11-03-08-02.pdf.

ISSN: 1678-4618
DOI: 10.26850/1678-4618eqj.v44.3.2019.p20-35

[18] The United States pharmacopeia. 36th revision: the national formulary. Washington DC: Rockville : United States Pharmacopeial Convention, 2013. 31st ed., 2013. ISBN: 9781936424122 1936424126.

[19] Allen, F. H., The Cambridge Structural Database: a quarter of a million crystal structures and rising, Acta Cryst. B (58) (2002) 380-388. https://doi.org/10.1107/S0108768102003890.

[20] Macrae, C. F., Bruno, I. J., Chisholm, J. A., Edgington, P. R., McCabe, P., Pidcock, E., Rodriguez-Monge, L., Taylor, R., van de Streek, J., Wood, P. A., Mercury CSD 2.0 - new features for the visualization and investigation of crystal structures, J. Appl. Cryst. 41 (2008) 466-470. https://doi.org/10.1107/S0021889807067908.

[21] Ng, W. K., Kwek, J. W., Yuen, A., Tan, C. L., Tan, R., Effect of milling on DSC thermogram of excipient adipic acid, AAPS PharmSciTech 11 (1) (2010) 159-167. https://doi.org/10.1208/s12249-009-9372-5.

[22] Moneghini, M., Kikic, I., Perissutti, B., Franceschinis, E., Cortesi, A., Characterisation of nimesulide–betacyclodextrins systems prepared by supercritical fluid impregnation, Eur. J. Pharm. Biopharm. 58 (2004) 637-644. https://doi.org/10.1016/j.ejpb.2004.04.004.

[23] Paiva, R. E. F., Abbehausen, C., Bergamini, F., Thompson, A., Antonini, A. D., Lancellotti, M., Corbi, P. P., Investigating the inclusion of the Ag(I)-nimesulide complex into β-cyclodextrin: studies in solution and in the solid state, J. Inc. Phenom. Macrocycl. Chem. 79 (1-2) (2014) 225-235. https://doi.org/10.1007/s10847-013-0348-4.

[24] Balasuwatthi, P., Dechabumphen, N., Saiwan, C., Scamehorn, J. F., Contact angle of surfactant solutions on precipitated surfactant surfaces. II. Effects of surfactant structure, presence of a subsaturated surfactant, pH, and counterion/surfactant ratio, J. Surf. Deterg. 7 (1) (2004) 31-40. https://doi.org/10.1007/s11743-004-0285-y.

[25] Puri, V., Dantuluri, A. K., Kumar, M., Karar, N., Bansal, A. K., Wettability and surface chemistry of crystalline and amorphous forms of a poorly water soluble drug, Eur. J. Pharm. Sci. 40 (2-12) (2010) 84-93. https://doi.org/10.1016/j.ejps.2010.03.003.

[26] Shete, G., Puri, V., Kumar, L., Bansal, A. K., Solid state characterization of commercial crystalline and amorphous atorvastatin calcium samples, AAPS PharmSciTech 11 (2) (2010) 598-609. https://doi.org/10.1208/s12249-010-9419-7.

[27] Vidal, N. L. G., Castro, S. G., Bruni, S. F. S., Allemandi, D. A., Palma, S. D., Albendazole solid dispersions: influence of dissolution medium composition on *in vitro* drug release, Dis. Technol. (2014) 42-47. https://doi.org/10.14227/DT210214P42.

[28] Park S. H., Choi H. K., The effects of surfactants on the dissolution profiles of poorly water-soluble acidic drugs, Int. J. Pharm. 32 (1-2) (2006) 35-41. https://doi.org/10.1016/j.ijpharm.2006.05.004.

[29] Shah, R. B., Tawakkul, M. A., Khan, M. A., Comparative evaluation of flow for pharmaceutical powders and granules, AAPS PharmSciTech 9 (1) (2008) 250-258. https://doi.org/10.1208/s12249-008-9046-8.

[30] Rigato, H. M., Borges, B. C., Sverdloff, C. E., Moreno, R. A., Orpineli, E., Borges, N. C., Bioavailability of two oral suspension and two oral tablet formulations of nimesulide 100 mg in healthy Brazilian adult subjects, Int. J. Clin. Pharm. Ther. 48 (3) (2010) 233-242. https://europepmc.org/abstract/med/20197019.

[31] Postali, M., Estudo de bioequivalência – proposição de um modelo animal em ratos para avaliação preditiva da biodisponibilidade de formulações contendo nimesulida em humanos. [dissertação]. Toledo (SC): Universidade Federal de Santa Catarina; 2011.

Eclética Química Journal, vol. 44, n. 3, 2019, 20-35
ISSN: 1678-4618
DOI: 10.26850/1678-4618eqj.v44.3.2019.p20-35

Eclética Química Journal

Original article
iq.unesp.br/ecletica

| Vol. 44 | n. 3 | 2019 |

Diketopiperazines and arylethylamides produced by *Schizophyllum commune*, an endophytic fungus in *Alchornea glandulosa*

Carolina Rabal Biasetto[1], Andressa Somensi[1], Fernanda Sales Figueiro[2], Luiz Alberto Beraldo de Moraes[2], Geraldo Humberto Silva[3], Maria Claudia Marx Young[4], Vanderlan da Silva Bolzani[1], Angela Regina Araújo[1+]

1 São Paulo State University (Unesp), Institute of Chemistry, 55 Prof. Francisco Degni Av., Araraquara, São Paulo, Brazil
2 University of São Paulo (USP), Faculty of Philosophy, Sciences and Letters, 3900 Bandeirantes Av., Ribeirão Preto, São Paulo, Brazil
3 Federal University of Viçosa (UFV), Institute of Science Exact and Technological, Peter Henry Rolfs Av., Viçosa, Minas Gerais, Brazil
4 São Paulo Institute of Botany, Nucleus of Research in Physiology and Biochemistry, 3687 Miguel Stéfano Av., São Paulo, São Paulo, Brazil

[+]Corresponding author: Angela Regina Araújo, email address: angela.araujo@unesp.br

ARTICLE INFO

Article history:
Received: December 5, 2018
Accepted: March 13, 2019
Published: July 4, 2019

Keywords:
1. Endophytic fungi
2. *Schizophyllum commune*
3. *Alchornea glandulosa*
4. diketopiperazines
5. arylethylamides

ABSTRACT: Chemical investigation of the crude PDB extract obtained from the endophytic fungus *Schizophyllum commune* afforded the pure substances, cyclo(*L*-Pro-*L*-Val) (1), uracil (2), cyclo(Pro-Tyr) (3), *p*-hydroxybenzoic acid (4) and a mixture of Rel.cyclo(Pro-Phe) (5) and Rel.cyclo(Pro-Ile) (6). When cultured in corn, the extract of this fungus yielded N-(2-phenylethyl) acetamide (7) and N-(4-hydroxyphenylethyl) acetamide (8). The structures of all compounds were determined based on the analyses of their MS, 1D and 2D-NMR spectroscopic data. Analysis of the crude extracts obtained from small-scale cultures (in PBD, YM, Nutrient, Czapek, Malt Extract, Corn and Rice) and a large-scale culture (in PDB) by mass spectrometry showed the presence of diketopiperazines 1, 3, 5 and 6. The crude extracts showed promising antioxidant, antifungal and acetylcholinesterase (AChE) inhibitory activities. The metabolites 7 and 8 showed antifungal and AChE inhibitory activities *in vitro*. This is the first report of the identification and isolation of diketopiperazines, arylethylamides, *p*-hydroxybenzoic acid in endophytic fungus of the *Schizophyllum* genus.

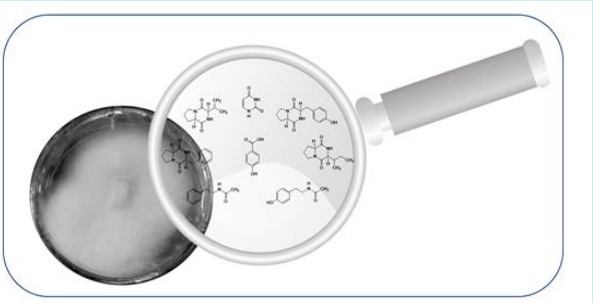

First report of the identification and isolation of diketopiperazines, arylethylamides and *p*-hydroxybenzoic acid in endophytic fungus of the *Schizophyllum* genus.

1. Introduction

Microorganisms as the endophytic fungi (endon = inside; phyton = plant) living asymptomatically in the intercellular space of host plants and establish a mutualistic relationship with its host during a part or all their life. These endophytes are found in parts of plants such as leaves, stems, fruits, seeds, and roots, and reside inside the plant all its life, being transmitted in some cases to future generations through seeds of the host[1-4]. The interactions established by endophytes may diversify from mutualism (endophyte and host plant obtain advantages) to parasitism (only the endophyte is benefited)[5,6]. Most natural products isolated from endophytes showed antimicrobial activity, and in many cases, these have been implicated in protecting the host plant against phytopathogenic microorganisms.[1,7,8] Studies in 2012 showed trichodermin and cercosporamide with strong antifungal and antitumor activities, which were isolated from endophyte belonging to the genus *Phoma* associated with *Arisaema erubescens*.[9]

Alchornea glandulosa (Euphorbiaceae) belongs to Brazilian Cerrado, which is well-known as

ISSN: 1678-4618
DOI: 10.26850/1678-4618eqj.v44.3.2019.p36-42

sources of bioactive secondary metabolites[10-13]. Several chemical and pharmacological studies were performed with extracts and pure substances from this plant and presented promising results[14-16]. Several endophytic fungi were isolated from this plant, including *S. commune*, which were chemically and biologically investigated. *S. commune* is a filamentous fungus belonging to the class of Basiodiomicetos, known as a producer of pigments, antiviral, anticancer and immunomodulatory compounds[17]. From this endophyte were isolated phenolic compounds as gallic acid and L-ascorbic acid, both with antioxidant activity[18]. Diketopiperazines present biological activities such as antiviral, antifungal, antibacterial, insecticidal, antihyperglycemic agents, receptor affinities of calcium channels and serotonergic[19-21]. Recent studies have demonstrated that diketopiperazine *trans*-cyclo(D-tryptophanyl-L-tyrosyl) presented low antiproliferative and cytotoxic effect with L-929 mouse fibroblast cells, K-562 leukemia cells and human HeLa Human cervix carcinoma[22]. Several arylethylamides present phytotoxic potential[23]. Thus, this work reports isolation, structural elucidation and biological activities of these compounds.

2. Materials and methods

2.1 General

NMR spectra were carried out one-dimensional ^{1}H Varian INOVA-300 spectrometer operating at 300 MHz for ^{1}H nucleus and TMS as internal reference. ^{1}H NMR spectra and ^{13}C 1D and 2D and NOESY 1D were performed on Varian INOVA-500 spectrometer operating at 500 MHz for ^{1}H nucleus and the nucleus 125 MHz for ^{13}C and TMS as internal reference. Mass spectra of high and low resolution were obtained on a spectrometer of UltrOTOFQ – ESI-TOF Mass Spectrometer (Bruker Daltonics, Billerica, MA, USA). Analyses were performed on a mass spectrometer with Varian 1200L LC autosampler, and triple-quadrupole electrospray ionization source (ESI). The mass spectra of low resolution were obtained on a LCQ Fleet spectrometer (Thermo Scientific) with electrospray ionization source (ESI). TLC was performed using Merck silica gel 60 G F_{254}. Spots on TLC plates were visualized under UV light and by spraying with anisaldehyde–H_2SO_4 reagent followed by heating at 120 °C. Analytical HPLC was performed on a Shimadzu (Shimadzu SPD-M20A) with diode array ultraviolet (DAD) detector, using a Phenomenex Gemini analytical column (C-18) (250 x 4.60 mm, 5 µm). Preparative HPLC was performed on Varian ProStar device coupled to the ProStar UV-Vis detector, using Phenomenex Luna C-18 silica semi-preparative column (150 x 21.20 mm; 5 µm). Optical rotation values were obtained at JASCO P-1020 polarimeter with sodium lamp, and 1.0 mL of cell Jasco Spectra Manager software.

2.2 Fungal isolation and identification

The traditional methodology[24] was used for the isolation of the endophytic fungus *S. commune* from healthy leaves of *Alchornea glandulosa*. *S. commune* was identified by sequencing and phylogenetic analysis of ribosomal operon gene fragments (CPQBA-UNICAMP-Multidisciplinary Center for Agricultural and Biological Chemistry Research, Campinas, Brazil). DNA sequence of the ITS region was analyzed using the GenBank BLAST routine and the CBS database (Centraalbureau voor Schimmelcultures, Fungal Biodiversity Centre).

The phylogenetic tree constructed from the sequences retrieved in GenBank and analyzes based on molecular data allowed the identification of this fungus as *Schizophyllum commune* (Filo Basidiomycota, order Agaricales and family Schizophyllaceae). The sequence of the isolate showed 99-98% similarity to sequences from different *S. commune* isolates, including *S. commune* BCC22128 and DSM 1025. In addition, in the phylogenetic tree, the isolate formed a cluster with the *S. commune* PRJ21 and 1-84 isolates supported by a bootstrap value of 94%. This endophytic fungus was stored in the NuBBE fungi collection in Araraquara, Brazil (kept in sterile water at 25 °C) encoded as Ag-Sc-02 and in CPQBA as CPQBA 154-09 DRM.

2.3 Cultivation

2.3.1 Different culture media (small scale)

S. commune was grown in Petri plates containing PDA (potato starch 4 g, dextrose 20 g, agar 15 g, H_2O 1000 mL) and incubated during ten days. After this period, this endophyte was cultivated in small scale in 2 Erlenmeyer flasks (500 mL) containing 300 mL of each liquid medium and these were autoclaved at 121 °C for

Eclética Química Journal, vol. 44, n. 3, 2019, 36-42
ISSN: 1678-4618
DOI: 10.26850/1678-4618eqj.v44.3.2019.p36-42

20 min. *S. commune* was cultivated in different liquid culture media (PBD, YM, Nutrient, Czapek, Malt Extract) under agitation at 120 rpm, for 28 days at 25 ℃. At the end of the incubation period, the broth was separated from the mycelium by filtration and the crude extracts were obtained by extraction with EtOAc (3 x 50% of the broth volume each) and dried in rotatory evaporator, affording 49.2, 54.0, 26.7, 26.5 and 38.2 mg, respectively. The cultivation on solid medium was performed: rice and corn inoculated in 2 Erlenmeyer flasks (500 mL each), containing each one: 90 g of rice or corn in 75 mL of Milli-Q H_2O. The culture media were autoclaved three times (three consecutive days) at 121 ℃ for 20 min. The cultures were incubated at 25 ± 2 ℃ for 21 days. At the end of the growth period, the solid cultures were ground and extracted with EtOAc (5x200 mL). The EtOAc fraction was subjected to liquid-liquid partition with H_2O. The EtOAc extract concentrated was dissolved in CH_3CN and then subjected to liquid-liquid partition with C_6H_{14}. The CH_3CN fractions were evaporated to give CH_3CN-deffated extracts, affording 279.7 (rice) and 335.1 (corn) mg.

2.3.2 PDB (large scale)

S. commune was inoculated in 52 Erlenmeyer flasks of 500 mL (large scale), containing each one: 1.2 g of potato starch, 6.0 g dextrose (PDB) in 300 mL of Milli-Q H_2O, which were autoclaved at 121 °C for 20 min. Approximately 5 small pieces (1x1 cm) of PDA medium, from the Petri dish containing biomass of the *S. commune* isolated were inoculated into Erlenmeyer flasks, sealed with cotton, to permit aerobic growth, and incubated at 25 ± 2 ℃ for 28 days. At the end of the incubation period, the cultures were combined, filtered, extracted with EtOAc (3x0.5 l). The solvent was evaporated, yielding a crude EtOAc extract (960 mg).

2.4 Purification and identification of chemical constituents

2.4.1 Liquid medium (PDB)

The EtOAc extract (960.0 mg) was fractioned by CC using reversed-phase silica gel (C-18) and gradient of H_2O:CH_3OH (15:100% CH_3OH (v/v)), resulting into eight fractions (*S.co*-F1-*S.co*-F8). The fraction *S.co*-F1 (559.0 mg) was further fractioned using reversed-phase silica gel (C-18) and eluted with a H_2O:CH_3OH gradient (35:100% CH_3OH (v/v), giving rise to seven subfractions (*S.co*-F1.1-*S.co*-F1.7). The subfraction *S.co*-F1.1 (470.0 mg) was fractioned by CC using reversed-phase silica gel (C-18) and gradient of H_2O:CH_3OH (5:100% CH_3OH (v/v)), resulting into seventeen fractions (*S.co*-F1.1.1-*S.co*-F1.1.17). Subfraction *S.co*-F1.1.2 was identified as cyclo(L-Pro-L-Val) (**1**) (16.0 mg). The subfraction *S.co*-F1.1.9 (2.0 mg) was analyzed by LC-MS (ACN:H_20 (05:95-50:50 v/v, 30'; 50:50-100:0 (v/v), 10'; 100:0-05:95 (v/v), 15'; 1 mL min^{-1} e λ=220 nm, C-18 column) and it was identified as cyclo(L-Pro-L-Val) (**1**), *Rel.cyclo*(Pro-Phe) (**5**) and *Rel.cyclo*(Pro-Ile) (**6**) (2.0 mg) in mixture. The fraction *S.co*-F1.1.1 (300.0 mg) was fractioned by CC using normal phase silica gel and gradient of $CHCl_3$:CH_3OH (2:100% CH_3OH (v/v) with 1% HOAc), resulting into fifty-five fractions (*S.co*-F1.1.1.1- *S.co*-F1.1.1.55). Subfraction *S.co*-F1.1.1.46 was isolated as compound uracil (**2**) (1.5 mg) and S.co-F1.1.1.38 was identified, in mixture, as cyclo(Pro-Tyr) (**3**) with *p*-hydroxybenzoic acid (**4**) (2.2 mg).

2.4.2 Solid medium (corn)

The CH_3CN-deffated extract (185.0 mg) was subjected to chromatography column (CC), normal phase (silica gel) by gradient elution with C_6H_{14}:EtOAc (70:30) (1 to 25% CH_3OH) affording into sixteen fractions (*S.co*-Mi1-*S.co*-Mi16). The subfractions *S.co*-Mi10 was identified as containing compound N-(2-phenylethyl) acetamide (**7**) (18.0 mg) and S.co-Mi16 was found to contain compound N-(4-hydroxyphenylethyl) acetamide (**8**) (20.0 mg).

2.5 Identification of diketopiperazines in different crude extracts

Analyses were performed on a mass spectrometer with Varian 1200L LC, direct insertion (ID) in positive mode. After the acquisition of information about protonated molecules by direct insertion, conducted experiments using MS-MS. Malt extract, Nutrient and YM (small scale) were subjected to MS-MS analysis in positive mode with application of 15 V collision energy.

2.6 Acetylcholinesterase inhibitory activity

Eclética Química Journal, vol. 44, n. 3, 2019, 36-42
ISSN: 1678-4618
DOI: 10.26850/1678-4618eqj.v44.3.2019.p36-42

The crude extracts (20 µg uL^{-1}) were eluted in TLC, being $CHCl_3$:CH_3OH (88:12) to the crude extract in liquid medium, Hexane: EtOAc (70:30) for the extracts in solid media. Compounds **7** and **8** (5 µg $µL^{-1}$) were applied on TLC layers, followed by elution with Hexane:EtOAc (70:30, v/v) and subsequent drying. The plates were then sprayed with enzyme solution (6.66 U mL^{-1}), thoroughly dried and incubated at 37 °C for 20 min (in a moist atmosphere). Enzyme activity was detected by spraying with a solution consisting of 0.25% 1-naphthyl acetate in CH_3CH_2OH containing 0.25% Fast Blue B salt (in aqueous solution). Potential acetylcholinesterase inhibitors appeared as clear zones on a purple-colored background. Electric eel AChE type V (product no. C 2888, 1000 U) and the other reagents were purchased from Sigma-Aldrich. The positive standard for comparison was physostigmine (0,05 µg mL^{-1})[25].

2.7 DPPH˙ scavenging capacity assay

Applied in microplates 96-well: 200 µL of DPPH (4 mg mL^{-1} in CH_3OH) and 100 µL of the samples at 7 different concentrations. Positive Control: 200 µL of DPPH and 100 µL of the standard antioxidant (quercetin and rutin). Negative control: 200 µL of DPPH and 100 µL of solvent. The microplate was kept for 30 minutes in the dark. The evaluation of the reduced form of DPPH generated by reading the absorbance at λ = 517 nm[26].

2.8 Evaluation of antifungal activity

The crude extracts (40 µg uL^{-1}) were eluted in TLC, being $CHCl_3$:CH_3OH (88:12) to the crude extract in liquid medium, Hexane: EtOAc (70:30 v/v) for the extracts in solid media. Compounds **7** and **8** (10 µg $µL^{-1}$) were applied on TLC layers, followed by elution with Hexane:EtOAc (70:30) and subsequent drying. The TLC layers were nebulized with the phypathogenic fungus Cladosporium cladosporioides (Fresen) and *C. sphaerospermum* (Perzig) SPC 491 (concentration of $5x10^7$ spores mL^{-1} in glucose solution and salts). The plates were incubated at 25 °C for 48 hours in absence of light. The positive standard for comparison was nystatin (1 µg)[27].

3. Results and discussion

The AcOEt extract of *S. commune* (PDB and corn) afforded compounds **1-8** (Figure 1) by using a combination of reversed (C-18) and normal phase (silica gel) chromatography. ^{1}H NMR and LC-MS analysis allowed to elucidate and identify the pure substances or in mixtures.

The known compounds cyclo(L-Pro-L-Val) (**1**), uracil (**2**), cyclo(Pro-Tyr) (**3**), *p*-hydroxybenzoic acid (**4**), *Rel.cyclo*(Pro-Phe) (**5**), *Rel.cyclo*(Pro-Ile) (**6**), N-(2-phenylethyl) acetamide (**7**) and N-(4-hydroxy phenylethyl) acetamide (**8**) were identified by comparing its spectroscopic data with literature values23,28-33. The spectrometric data ^{1}H NMR and MS of the culture medium without *S. commune* were compared with the spectra of the compound and showed no similarity.

The substance **7** showed low potential to inhibit the enzyme acetylcholinesterase and strong activity against *C. cladosporioides*. The substance **8** showed moderate potential to inhibit the enzyme acetylcholinesterase and weak activity against *C. cladosporioides* and *C. sphaerospermum.*

The crude extracts showed promising results for biological assays as antioxidant, highlighting the Malt Extract with a significant DPPH˙ sequestration rate of 68.36% and IC_{50}= 28.7 µg mL^{-1}, compared to IC_{50}= 7.49 µg L^{-1} standard quercetin. The majority these extracts exhibited strong antifungal activity against the phytopathogenic fungi *C. cladosporioides* and *C. sphaerospermum*. The crude extracts displayed moderate AChE inhibitory activity. Unfortunately, the substances responsible by these bioactivities were not isolated.

The diketopiperazines **1**, **3**, **5** and **6** were detected in PDB extract (small scale) by MS. The crude extracts obtained from YM, Nutrient and Malt were subjected to MS-MS analysis and indicated the presence of diketopiperazines **1**, **5** and **6**. Analysis of crude extracts by direct insertion (ID), showed the protonated diketopiperazines and their fragments in five crude extracts by MS-MS experiment, which corroborate with the fragmentation characteristic of diketopiperazines isolated or identified in mixture.

In the crude extracts Czapek, rice (CH_3CN) and corn (CH_3CN) (small scale) the diketopiperazines were not identified, suggesting that the enzymes responsible by the biosynthesis of these compounds were not expressed by *S. commune*, in these media. With these observations was possible to confirm that the culture media influences the microorganisms metabolic production.

Eclética Química Journal, vol. 44, n. 3, 2019, 36-42
ISSN: 1678-4618
DOI: 10.26850/1678-4618eqj.v44.3.2019.p36-42

cyclo(L-Pro-L-Val) (**1**)
ESIMS *m/z* 197.0 $[M+H]^+$ and fragments: 169.0 $[M+H-28]^+$, 124.5 $[M+H-73]^+$, 70.0 $[M+H-127]^+$.

cyclo(L-Pro-L-Tyr) (**3**)
ESIMS *m/z* 261.3 $[M+H]^+$ and fragments: 233.0 $[M+H-28]^+$, 121.0 $[M+H-140]^+$, 136.0 $[M+H-125]^+$, 70.3 $[M+H-191]^+$.

Rel.cyclo(Pro-Phe) (**5**)
ESIMS *m/z* 245.5 $[M+H]^+$ and fragments: 217.0 $[M+H-28]^+$, 154.1 $[M+H-90]^+$, 70.0 $[M+H-175]^+$.

Rel.cyclo(Pro-Ile) (**6**)
ESIMS *m/z* 211.5 $[M+H]^+$ and fragments: 183.0 $[M+H-28]^+$, 137.8 $[M+H-73]^+$, 114.1 $[M+H-97]^+$, 69.6 $[M+H-141]^+$.

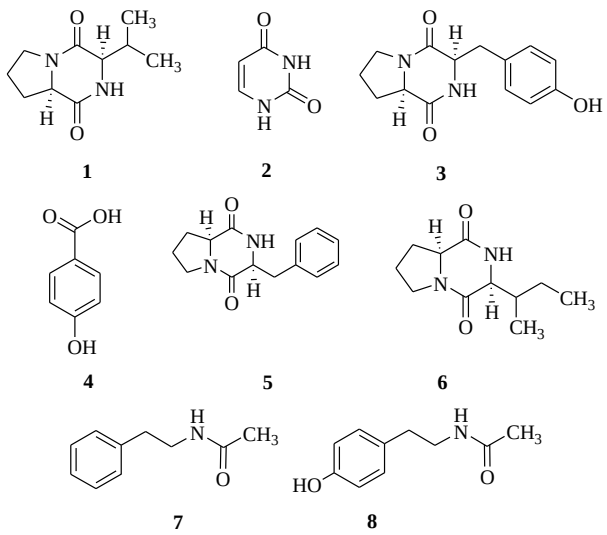

Figure 1. Compounds produced by the endophytic fungus *S. commune*.

4. Conclusions

The present study was designed to be the most comprehensive investigation of chemical constituents in *S. commune*. This is the first report of the identification and isolation of diketopiperazines, arylethylamides, *p*-hydroxybenzoic acid in endophytic fungus of the *Schizophyllum* genus. Diketopiperazines was observed by mass spectrometry in the different crude extracts in small scale and PDB large scale, indicating this endophyte as a prolific producer of class of compounds by variation of nutrients of culture media. The biological activities reported by the compounds produced by *S. commune* suggest an ecological interaction, as well as in the plant protection as a defense mechanism of other organisms that inhabit the plant species.

These results reinforce the potential of these microorganisms as sources of secondary metabolites and collaborating with understanding the endophytic interaction and its host plant.

First attempts made to correlate variations in bands assigned as carbonyl stretching frequencies in the infrared region for solid metal ion complexes with the stability constants of these same complexes in solution date back to early 1950s.

5. References

[1] Gunatilaka, A. A. L., Natural products from plant-associated microorganisms: distribution, structural diversity, bioactivity, and implications of their occurrence, J. Nat. Prod. 69 (3) (2006) 509-526. https://doi.org/10.1021/np058128n.

[2] Rodriguez, R. J., White Jr. J. F., Arnold, A. E., Redman, R. S., Fungal endophytes: diversity and functional roles, New Phytologist 182 (2) (2009) 314-330. https://doi.org/10.1111/j.1469-8137.2009.02773.x.

[3] Tan, R. X., Zou, W. X., Endophytes: a rich source of functional metabolites, Nat. Prod. Rep. 18 (8) (2001) 448-459. https://doi.org/10.1039/B100918O.

[4] Kusari, S., Pandey, S. P., Spiteller, M., Untapped mutualistic paradigms linking host plant and endophytic fungal production of similar bioactive secondary metabolites, Phytochemistry 91 (2013) 81-87. https://doi.org/10.1016/j.phytochem.2012.07.021.

[5] Bae, H., Sicher, R. C.; Kim, M. S., Kim, S-H.; Strem, M. D., Melnick, R. L., Bailey, B. A., The beneficial endophyte *Trichoderma hamatum* isolate DIS 219b promotes growth and delays the onset of the drought response in *Theobroma cacao*, J. Exp. Bot. 60 (11) (2009) 3279-3295. https://doi.org/10.1093/jxb/erp165.

[6] Kusari, P., Kusari, S., Spiteller, M., Kayser, O., Implications of endophyte-plant crosstalk in light of quorum responses for plant biotechnology, Appl. Microbiol. Biotechnol. 99 (13) (2015) 5383-5390. https://doi.org/10.1007/s00253-015-6660-8.

[7] Gutierrez, R. M. P., Gonzalez, A. M. N., Ramirez, A. M., Compounds derived from endophytes: a review of phytochemistry and pharmacology, Curr. Med. Chem. 19 (18) (2012) 2992-3030. https://doi.org/10.2174/092986712800672111.

Eclética Química Journal, vol. 44, n. 3, 2019, 36-42
ISSN: 1678-4618
DOI: 10.26850/1678-4618eqj.v44.3.2019.p36-42

[8] Kusari, S., Spiteller, M., Are we ready for industrial production of bioactive plant secondary metabolites utilizing endophytes? Nat. Prod. Rep. 28 (7) (2011) 1203-1207. https://doi.org/10.1039/c1np00030f.

[9] Wang, L. W., Xu, B. G., Wang, J. Y., Su, Z. Z., Lin, F. C., Zhang, C. L., Kubicek, C. P., Bioactive metabolites from Phoma species, an endophytic fungus from the Chinese medicinal plant *Arisaema erubescens*, Appl. Microbiol. Biot 93 (3) (2012) 1231-1239. https://doi.org/10.1007/s00253-011-3472-3.

[10] Bolzani, V. S., Trevisan, L. M. V., Young, M. C. M., Caffeic acid esters and triterpenes of *Alibertia macrophyla*. Phytochemistry 30 (6) (1991) 2089-2091. https://doi.org/10.1016/0031-9422(91)85077-D.

[11] Young, M. C. M., Braga, M. R., Dietrich, S. M. C., Gottlieb, H. E., Trevisan, L. M. V., Bolzani, V. S., Fungitoxic non-glycosidic iridoids from *Alibertia macrophylla*, Phytochemistry 31 (10) (1992) 3433-3435. https://doi.org/10.1016/0031-9422(92)83701-Y.

[12] Silva, V. C., Faria, A. O., Bolzani, V. S., Lopes, M. N., A new *ent*-kaurane diterpene from stems of *Alibertia macrophylla* K. SCHUM. (Rubiaceae), Helv. Chim. Acta 90 (10) (2007) 1781-1785. https://doi.org/10.1002/hlca.200790187.

[13] Junior, C. V., Pivatto, M., Rezende, A., Hamerski, L., Silva, D. H. S., Bolzani, V. S., (–)-7-Hydroxycassine: a new 2,6-dialkylpiperidin-3-ol alkaloid and other constituents isolated from flowers and fruits of *Senna spectabilis* (Fabaceae), J. Braz. Chem. Soc. 24 (2) (2013) 230-235. https://doi.org/10.5935/0103-5053.20130029.

[14] Calvo, T. R., Lima, Z. P., Silva, J. S., Ballesteros, K. V. R., Pellizzon, C. H., Hiruma-Lima, C. A., Tamashiro, J., Brito, A. R. M. S., Takahira, R. K., Vilegas, W., Constituents and antiulcer effect of *Alchornea glandulosa*: activation of cell proliferation in gastric mucosa during the healing process, Biol. Pharm. Bull. 30 (3) (2007) 451-459. https://doi.org/10.1248/bpb.30.451.

[15] Conegero, L. S., Ide, R. M., Nazari, A. S., Sarragiotto, M. H., Filho, B. P. D., Nakamura, C. V., Carvalho, J. E., Foglio, M. A., Constituintes químicos de *Alchornea glandulosa* (Euphorbiaceae), Quím. Nova 26 (6) (2003) 825-827. https://doi.org/10.1590/S0100-40422003000600008.

[16] Lopes, F. C. M., Rocha, A., Pirraco, A., Regasini, L. O., Silva, D. H. S., Bolzani, V. S., Azevedo, I., Carlos, I. Z., Soares, R., Anti-angiogenic effects of pterogynidine alkaloid isolated from *Alchornea glandulosa*, BMC Complem. Altern. M. 9 (15) (2009). https://doi.org/10.1186/1472-6882-9-15.

[17] Kumari, M., Survase, S. A., Singhal, R. S., Production of schizophyllan using *Schizophyllum commune* NRCM, Bioresource Technol. 99 (5) (2008) 1036-1043. https://doi.org/10.1016/j.biortech.2007.02.029.

[18] Tripathi, A. M., Tiwary, B. N., Biochemical constituents of a wild strain of *Schizophyllum commune* isolated from Achanakmar-Amarkantak Biosphere Reserve (ABR), India, World Journal of Microbiology and Biotechnology 29 (8) (2013) 1431-1442. https://doi.org/10.1007/s11274-013-1306-4.

[19] Martins, M. B., Carvalho, I., Diketopiperazines: biological activity and synthesis, Tetrahedron 63 (40) (2007) 9923-9932. https://doi.org/10.1016/j.tet.2007.04.105.

[20] Gendy, B. D. M., Rateb, M. E., Antibacterial activity of diketopiperazines isolated from a marine fungus using *t*-butoxycarbonyl group as a simple tool for purification, Bioorg. Med. Chem. Lett. 25 (15) (2015) 3125-3128. https://doi.org/10.1016/j.bmcl.2015.06.010.

[21] Sathya, A., Vijayabharathi, R., Kumari, B. R., Srinivas, V., Sharma, H. C., Sathayadevi, P., Gopalakrishnan, S., Assessment of a diketopiperazine, cyclo(Trp-Phe) from *Streptomyces griseoplanus* SAI 25 against cotton bollworm, *Helicoverpa armigera* (Lepidoptera: Noctuidae), Appl. Entomol. Zool. 51 (1) (2016) 11-20. https://doi.org/10.1007/s13355-015-0366-3.https://doi.org/10.1007/s13355-015-0366-3

[22] Ivanova, V., Laatsch, H., Kolarova, M., Aleksieva, K., Structure elucidation of a new natural diketopiperazine from a *Microbispora aerata* strain isolated from Livingston Island, Antarctica, Nat. Prod. Res. 27 (2) (2013) 164-170. https://doi.org/10.1080/14786419.2012.665911.

[23] Maskey, R. P., Asolkar, R. N.; Kapaun, E., Wagner-Döbler, I., Laatsch, H., Phytotoxic arylethylamides from limnic bacteria using a screening with microalgae, J. Antibiotics 55 (7) (2002) 643-649. https://doi.org/10.7164/antibiotics.55.643.

[24] Teles, H. L., Silva, G. H., Castro-Gamboa, I., Bolzani, V. S., Pereira, J. O., Costa-Neto, C. M., Eberlin, M. N., Young, M. C. M., Araújo, A. R., Benzopyrans from *Curvularia* sp., an endophytic fungus associated with *Ocotea corymbosa* (Lauraceae), Phytochemistry 66 (19) (2005) 2363-2367. https://doi.org/10.1016/j.phytochem.2005.04.043.

ISSN: 1678-4618
DOI: 10.26850/1678-4618eqj.v44.3.2019.p36-42

[25] Marston, A., Kissling, J., Hostettmann, K., A rapid TLC bioautographic method for the detection of acetylcholinesterase and butyrylcholinesterase inhibitors in plants, Phytochem. Analysis 13 (1) (2002) 51-54. https://doi.org/10.1002/pca.623.

[26] Pauletti, P. M., Castro-Gamboa, I., Silva, D. H. S., Young, M. C. M., Tomazela, D. M., Eberlin, M. N., Bolzani, V. S., New antioxidant C-glucosylxanthones from the stems of *Arrabidaea samydoides*, J. Nat. Prod. 66 (10) (2003) 1384-1387. https://doi.org/10.1021/np030100t.

[27] Rahalison, L., Hamburger, M., Hostettmann, K., Monod, M., Frenk, E., A bioautographic agar overlay method for the detection of antifungal compounds from higher plants, Phytochem. Analysis 2 (5) (1991) 199-203. https://doi.org/10.1002/pca.2800020503.

[28] Fdhila, F., Vázquez, V., Sánchez, J. L., Riguera, R., DD-Diketopiperazines: antibiotics active against *Vibrio anguillarum* isolated from marine bacteria associated with cultures of *Pectenmaximus*, J. Nat. Prod., 66 (10) (2003) 1299-1301. https://doi.org/10.1021/np030233e.

[29] Jayatilake, G. S., Thornton, M. P., Leonard, A. C., Grimwade, J. E., Baker, B. J., Metabolites from an Antarctic sponge-associated bacterium, *Pseudomonas aeruginosa*, J. Nat. Prod. 59 (3) (1996) 293-296. https://doi.org/10.1021/np960095b.

[30] Lin, Z. J., Lu, X. M., Zhu, T. J., Fang, Y. C., Gu, Q. Q., Zhu, W., GPR12 Selections of the metabolites from an endophytic *Streptomyces* sp. associated with *Cistanches deserticola*, Arch Pharm. Res. 31 (1108) (2008) 1108-1114. https://doi.org/10.1007/s12272-001-1276-4.

[31] Marinho, A. M. R., Marinho, P. S. B., Rodrigues, E. F., Chemical components of *Penicillium* sp, an endophytic fungus from *Murraya paniculata* (Rutaceae), Revista Ciências Exatas e Naturais 9 (2) (2007) 189-199. https://revistas.unicentro.br/index.php/RECEN/article/view/80.

[32] Takaya, Y., Furukawa, T., Miura, S., Akutagawa, T., Hotta, Y., Ishikawa, N., Niwa, M., Antioxidant constituents in distillation residue of awamori spirits, J. Agric. Food Chem. 55 (1) (2007) 75-79. https://doi.org/10.1021/jf062029d.

[33] Wang, G., Dai, S., Chen, M., Wu, H., Xie, L., Luo, X., Li, X., Two diketopiperazine cyclo(pro-phe) isomers from marine bacteria *Bacillus subtilis* sp. 13-2, Chem. Nat. Compd. 46 (4) (2010) 583-585. https://doi.org/10.1007/s10600-010-9680-8.

Eclética Química Journal, vol. 44, n. 3, 2019, 36-42
ISSN: 1678-4618
DOI: 10.26850/1678-4618eqj.v44.3.2019.p36-42

Eclética Química Journal

Original article
iq.unesp.br/ecletica

| Vol. 44 | n. 3 | 2019 |

Application of a ternary phase diagram to the liquid-liquid extraction of ethanoic acid using ethyl ethanoate

Aline Amaral Madeira+

Pontifical Catholic University of Minas Gerais (PUC-MG), 500 Dom José Gaspar Av, Belo Horizonte, Minas Gerais, Brazil

+ Corresponding author: Aline Amaral Madeira, email address: madeira.alineamaral@gmail.com

ARTICLE INFO

Article history:
Received: January 21, 2019
Accepted: March 9, 2019
Published: July 4, 2019

Keywords:
1. ethanoic acid
2. liquid-liquid extraction
3. ternary phase diagram
4. binodal curve
5. tie-lines

ABSTRACT: This article describes the liquid-liquid equilibrium of the extraction process of ethanoic acid ($C_2H_4O_2$) in aqueous phase using ethyl ethanoate as the solvent. The liquid-liquid extraction was modeled by the construction of a ternary phase diagram for the water/ethanoic acid/ethyl ethanoate system using the Origin software. The equilibrium data were experimentally obtained by titration at room temperature (298.15 K) and atmospheric pressure (101325 Pa) using four mixtures of water, ethanoic acid, and ethyl ethanoate. The determination of the composition of the extract and residue portions in the equilibrium of each mixture by of the tie-lines method allowed to examine the percentages of liquid-liquid extraction achieved. The distribution coefficients and separation factors calculated, made it possible an evaluation of the distribution and of the mutual solubility of the solute in the aqueous and organic phases. The results showed a good performance of ethyl ethanoate in the extraction of ethanoic acid for concentrations of solute until 16% of the feed.

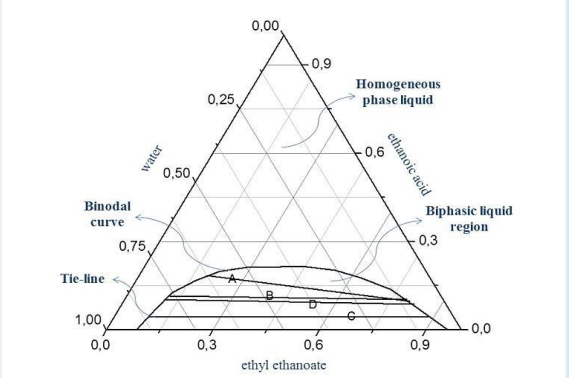

Ternary phase diagram for the water-ethanoic acid-ethyl ethanoate system

1. Introduction

Ethanoic acid ($C_2H_4O_2$) is one of the most widely used and important carboxylic acids in the world. Its wide range of applications includes its use as a raw material in the production of polymers derived from vinyl acetate, purified terephthalic acid, and esters of acetic anhydride and acetate, and as a solvent in the production of cellulose acetate and in the manufacture of pharmaceutical products[1,2]. Its global market demand was 13 million tons in 2015 and is forecast to reach 18 million tons by 2020[3].

The separation of the mixture of ethanoic acid and water is of great economic importance but is particularly difficult because it forms a pinch azeotrope. It is not a real azeotropic mixture, but the equilibrium concentrations of its constituents are very close and therefore requires many stages. For mixtures with concentrations below 40% ethanoic acid, the liquid-liquid extraction process is the most appropriate[1].

Liquid-liquid extraction (LLE) is an important unitary operation employed in the chemical industry due to its high efficiency and low energy consumption and environmental impact. It is one of the most important mass transfer processes in chemical engineering and an alternative method to distillation[4]. Its efficiency is based on the physical and chemical properties of a solvent (organic phase) used to separate, purify or concentrate a certain constituent of an aqueous phase[5,6].

To design and optimize the LLE, liquid-liquid equilibrium data provided by ternary phase diagrams involving a solubility curve and tie-lines are required[5]. From the industrial point of view,

Eclética Química Journal, vol. 44, n. 3, 2019, 43-49
ISSN: 1678-4618
DOI: 10.26850/1678-4618eqj.v44.3.2019.p43-49

knowledge of phase equilibrium is essential in modern process design and control methods[4]. Liquid-liquid equilibrium studies of systems composed of water, phenolic compounds and organic solvents are necessary for the evaluation of industrial units for solvent extraction processes[7].

The equilibrium behavior of a three-component liquid-liquid system is typically described using a ternary phase diagram where experimental solubility data are plotted as points, which in turn lie in the binodal curve. The ternary phase diagram consists of an equilateral triangle where each side is divided into equal parts, corresponding to the mass fractions of each component of the system. The sides of the triangle represent the binary mixtures, while the vertices correspond to the pure components. Within the binodal curve, the biphasic liquid region is located, as well as the tie-lines that join the extract and residue streams in equilibrium, and outside, the homogeneous phase region[8-10].

The spectrum of potential solvents for separation processes involving liquid-liquid extraction includes ethyl ethanoate, which has excellent properties for industrial applications, as well as being environmentally friendly and low cost, low toxicity and chemical stability[11]. Ethyl ethanoate has low toxicity compared to most organic solvents (benzene, toluene, chloroform) and its saturation temperature is considerably lower than other low toxicity solvents[12].

In this context, based with the increasing worldwide demand for ethanoic acid, as well as in advantages of the use of ethyl ethanoate, the present article aims at studying the application of ternary phase diagram to the liquid-liquid extraction of ethanoic acid from aqueous phase using ethyl ethanoate as the solvent.

2. Materials and methods

2.1 Binodal curve construction

The liquid-liquid extraction process of ethanoic acid ($C_2H_4O_2$) realized was modeled by the construction of a ternary phase diagram for the water/ethanoic acid/ethyl ethanoate system at room temperature (298.15 K) and atmospheric pressure (101325 Pa). Initially, six points of the binodal curve for the water-rich phase were created by titration with ethyl ethanoate using 25.00 mL of water and the volumes of 0.00; 2.00; 4.00; 6.00; 8.00, and 10.00 mL of ethanoic acid in each point. The volumes of ethyl ethanoate, required for the turbidity of the aqueous solution containing ethanoic acid, were experimentally obtained and presented in Table 1. Subsequently, more seven points were created for the ethyl ethanoate-rich phase. For this, 25.00 mL of ethyl ethanoate and 0.00; 2.00; 4.00; 6.00; 8.00, 10.00 and 12.00 mL of ethanoic acid were used. The water expenses volumes were presented in Table 2.

Table 1. Experimental data of water-rich phase at T = 298.15 K under P = 101325 Pa.

Point	Volumes (mL)		
	Water	Ethanoic acid	Ethyl ethanoate
1	25.00	0.00	2.50
2		2.00	3.50
3		4.00	4.50
4		6.00	7.00
5		8.00	10.40
6		10.00	15.90

Table 2. Experimental data of ethyl ethanoate-rich phase at T = 298.15 K under P = 101325 Pa.

Point	Volumes (mL)		
	Ethyl ethanoate	Ethanoic acid	Water
7	25.00	0.00	0.90
8		2.00	2.40
9		4.00	4.00
10		6.00	7.00
11		8.00	10.60
12		10.00	16.40
13		12.00	23.80

2.2 Tie-lines obtention

Four mixtures (A, B, C, and D) were prepared using the volumes of water, ethanoic acid, and ethyl ethanoate described in Table 3. The preparation of each them was realized with magnetic agitation for 10 minutes at room temperature (298.15 K). Then, each mixture was submitted to one stage of extraction, compound by contact and separation. The ternary systems were made in contact by vigorous agitation in a separation funnel of 60.0 mL and were kept in repose for 5 minutes. The aqueous and organic phases were separated for a posterior measure of mass and volume. Aliquots of 5.00 mL of each phase were titrated with sodium hydroxide solution (NaOH) 1 mol L^{-1} using 3,3-bis(4-hydroxyphenyl)-2-benzofuran-1-one ($C_{20}H_{14}O_4$) as the indicator.

Eclética Química Journal, vol. 44, n. 3, 2019, 43-49
ISSN: 1678-4618
DOI: 10.26850/1678-4618eqj.v44.3.2019.p43-49

The volumes of NaOH expensed in each titration were presented in Table 4.

Table 3. Data survey for tie-lines obtention.

Component	Volumes of the mixtures (mL)			
	A	B	C	D
Ethyl ethanoate	25.00	25.00	25.00	25.00
Ethanoic acid	8.00	5.00	2.00	4.00
Water	17.00	20.00	23.00	21.00

Table 4. Titration data of the mixtures A, B, C, and D at T = 298.15 K under P = 101325 Pa.

Mixture	Aqueous phase				Organic phase			
	volume (mL)	mass (g)	volume NaOH (mL)	mols NaOH/10^{-3} (5 mL)	volume (mL)	mass (g)	volume NaOH (mL)	mols NaOH/10^{-3} (5 mL)
A	17.00	15.79	14.30	14.30	33.00	30.47	14.40	14.40
B	21.50	21.02	9.40	9.40	25.00	23.08	9.10	9.10
C	25.00	24.26	3.60	3.60	25.00	23.07	3.30	3.30
D	25.00	22.47	7.73	7.73	26.00	24.05	7.00	7.00

2.3 Plotting the equilibrium data

The ternary phase diagram of water/ethanoic acid/ethyl ethanoate system was built using the Origin® software from of equilibrium data obtained in items 2.1 and 2.2. The volumes were converted in mass using the densities of each component at 298.15 K ($\rho_{ethanoic\ acid}$ = 1.052 g mL^{-1}; $\rho_{ethyl\ ethanoate}$ = 0.901 g mL^{-1}; and ρ_{water} = 0.997 g mL^{-1}). The diagram was used to study the liquid-liquid extraction process of ethanoic acid ($C_2H_4O_2$) from aqueous phase with the use of ethyl ethanoate as the solvent.

3. Results and discussion

The equilibrium compositions in the binodal curve (in mass fraction) for each component of the water/ethanoic acid/ethyl ethanoate system at 298.15 K and 101325 Pa were given in Table 5. The same results were plotted in Figure 1. The area of the biphasic liquid region obtained results from the mutual solubility of the solute (ethanoic acid) in the aqueous and organic solvent (ethyl ethanoate).

Table 5. Mass fractions of the compounds of the ternary system at T = 298.15 K under P = 101325 Pa.

Phase	Binodal curve point	Water	Ethyl ethanoate	Ethanoic acid
Water-rich	1	0.9171	0.0829	0
	2	0.8258	0.1045	0.0697
	3	0.7510	0.1222	0.1268
	4	0.6639	0.1680	0.1681
	5	0.5836	0.2194	0.1970
	6	0.5008	0.2878	0.2114
Ethyl ethanoate-rich	7	0.4030	0.3826	0.2144
	8	0.3310	0.4560	0.2130
	9	0.2546	0.5427	0.2028
	10	0.1949	0.6289	0.1762
	11	0.1298	0.7332	0.1370
	12	0.0886	0.8336	0.0779
	13	0.0383	0.9617	0

Eclética Química Journal, vol. 44, n. 3, 2019, 43-49
ISSN: 1678-4618
DOI: 10.26850/1678-4618eqj.v44.3.2019.p43-49

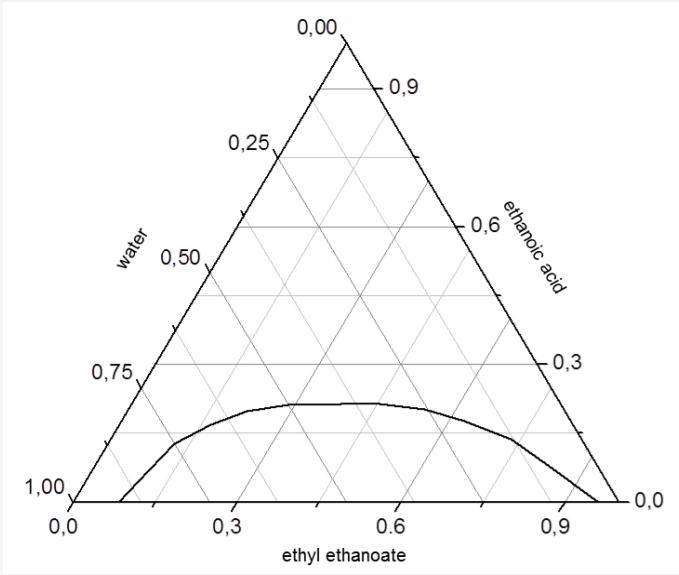

Figure 1. Ternary phase diagram of water/ethanoic acid/ethyl ethanoate system with binodal curve at T = 298.15 K under P = 101325 Pa.

The titration reaction involved in the volumetric analysis of ethanoic acid determination in each of the phases of the mixtures A, B, C, and D was presented in Equation 1. Since the reaction is 1:1, at the point of equivalence, the molar amount of ethanoic acid was equal to the sodium hydroxide. The formation of the reaction product, the acetate conjugate base (CH_3COO^-), was easily identified by the use of the indicator 3,3-bis (4-hydroxyphenyl)-2-benzofuran-1-one ($C_{20}H_{14}O_4$), which has a transition zone in the alkaline region.

$$CH_3COOH + OH^- \leftrightarrow CH_3COO^- + H_2O \qquad (1)$$

The mass fractions of ethanoic acid (MW 60.052 g mol^{-1}), calculated from the equivalence of the number of moles of sodium hydroxide, as well as the mass fractions for the other components of the ternary system, found directly in the obtained diagram, were given in Table 6. The results obtained were plotted in Figure 2, where the tie-lines of each mixture were drawn.

Table 6. Mass fractions of the tie-lines of the ternary system at T = 298.15 K under P = 101325 Pa.

Mixture	Aqueous phase			Organic phase		
	Ethanoic acid	Water	Ethyl ethanoate	Ethanoic acid	Water	Ethyl ethanoate
A	0.1849	0.6253	0.1905	0.0965	0.0978	0.8055
B	0.1155	0.7652	0.1201	0.1018	0.1026	0.7928
C	0.0446	0.8558	0.0973	0.0430	0.0680	0.8890
D	0.1033	0.7849	0.1126	0.0874	0.0907	0.8225

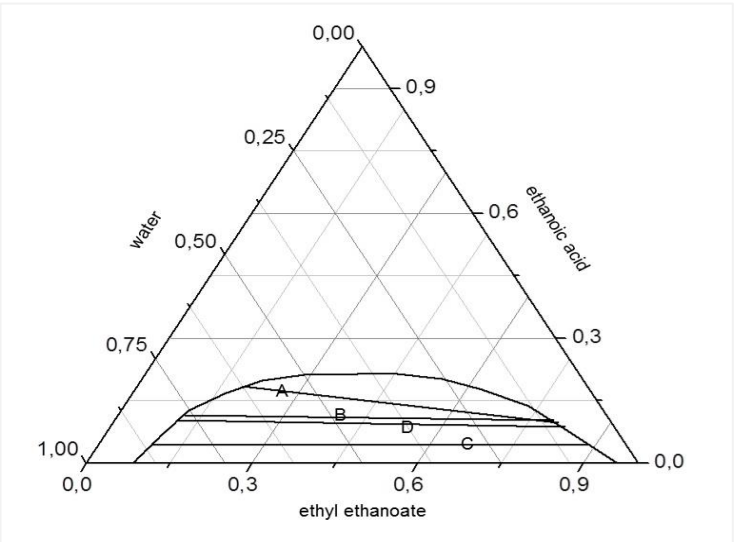

Figure 2. Ternary phase diagram of water/ethanoic acid/ethyl ethanoate system with the tie-lines corresponding to mixtures A, B, C, and D at T = 298.15 K under P = 101325 Pa.

Eclética Química Journal, vol. 44, n. 3, 2019, 43-49
ISSN: 1678-4618
DOI: 10.26850/1678-4618eqj.v44.3.2019.p43-49

The results obtained in the study of liquid-liquid extraction for the water/ethyl ethanoate/ethanoic acid ternary system were summarized in Figure 3. The ethyl ethanoate free-base feed composition was represented by F point (water/ethanoic acid/ethyl ethanoate = 0.84/0.16/0) and extractor solvent (pure) was represented by B point (water/ethanoic acid/ethyl ethanoate = 0/0/1). The intersection between the FB segment and the tie-line corresponding to the D mixture was represented by the M point, which in turn binds the extract (E) and residue (R) phases in equilibrium in the binodal curve. The equilibrium composition of the E and R phases in the mass fraction of ethanoic acid was of Y_e = 0.098 and X_r = 0.102, respectively.

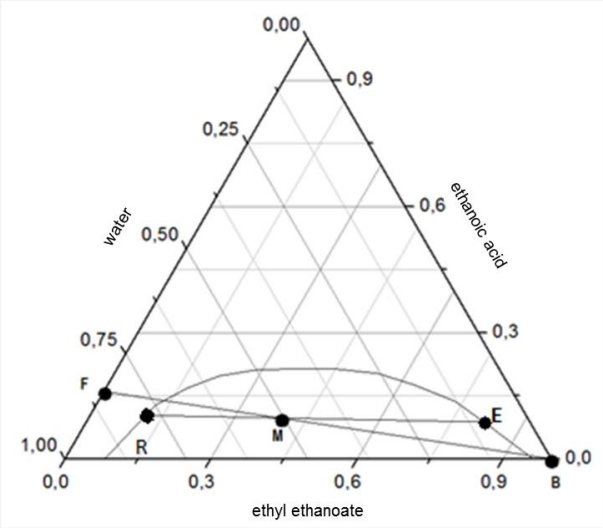

Figure 3. Ternary phase diagram of water/ethanoic acid/ethyl ethanoate system for mixture D at T = 298.15 K under P = 101325 Pa (where F: feed; B: solvent; M: F + B mixture; E: extract, and R: residue).

The distribution coefficients (D) and the separation factors (S) for mixtures A, B, C, and D were calculated to evaluate the efficacy of extraction of ethanoic acid by the organic solvent (ethyl ethanoate) by Equation 2. The separation factor, which is a measure of the ability of a solvent to separate a solute from water, was defined as the ratio between the ethanoic acid (D_2) and water (D_1) distribution coefficients, respectively. The experimental values of the distribution coefficients and separation factors, for each mixture of the ternary system, were listed in Table 7.

$$S = \frac{D_2}{D_1} = \frac{x_{EA,EE}/x_{EA,W}}{x_{W,EE}/x_{W,W}} \quad (2)$$

where:
S = separation factor;
D_1 = distribution coefficients for water;
D_2 = distribution coefficient for ethanoic acid;
$x_{EA,EE}$ = mass fraction of ethanoic acid in the ethyl ethanoate-rich phase;
$x_{EA,W}$ = mass fraction of ethanoic acid in the water-rich phase;
$x_{W,EE}$ = mass fraction of water in the ethyl ethanoate-rich phase;
$x_{W,W}$ = mass fraction of water in the water-rich phase.

Table 7. Distribution coefficients for water (D_1) and ethanoic acid (D_2) and separation factors (S) at T = 298.15 K under P = 101325 Pa.

System	Mixture	D_1	D_2	S
Water + Ethanoic acid + Ethyl ethanoate	A	0.16	0.52	3.34
	B	0.13	0.88	6.57
	C	0.08	0.96	12.13
	D	0.12	0.85	7.32

The organic solvent chosen was found to have shown satisfactory separation factors (i.e. > 1), indicating its ability to extract ethanoic acid from water. The results demonstrated that the separation factor decreases in the order of the mixtures C > D > B > A. For the ternary system, increasing the ethanoic acid content in the mixtures decreased the separating ability of ethyl ethanoate. The ethanoic acid distribution coefficients showed values higher than the water distribution coefficients, suggesting a higher preference of the solute to be distributed in the organic phase than in the aqueous phase.

The percentages liquid-liquid extraction (%LLE) of ethanoic acid in water were determined for each mixture by tie-lines method and Equation 3 and can be checked in Table 8. The results suggested that the percentage extraction decreases in the order of the mixtures D > B > C > A, indicating that, for concentrations of ethanoic acid greater than 16% in F, there was a reduction in the solvent extraction capacity. In short, ethyl ethanoate showed good performance in extracting ethanoic acid from the aqueous phase of the mixtures.

$$\%LLE = \left(\frac{x_F F - x_R R}{x_F F}\right) x\ 100 \quad (3)$$

Eclética Química Journal, vol. 44, n. 3, 2019, 43-49
ISSN: 1678-4618
DOI: 10.26850/1678-4618eqj.v44.3.2019.p43-49

where:
x_F = feed mass fraction;
x_R = residue mass fraction;
F = feed mass;
R = residue mass.

Table 8. Percentage liquid-liquid extraction (%LLE) of ethanoic acid in the mixtures A, B, C, and D

Mixture	x_F	x_M	x_R	y_E	F	M	R	E	$\%LLE$
A	0.3318	0.1757	0.1849	0.0965	25.3650	47.8900	42.9255	4.9645	5.69
B	0.2087	0.1102	0.1155	0.1018	25.2000	47.7250	29.3135	18.4115	35.63
C	0.0840	0.0442	0.0446	0.0430	25.0350	47.5600	36.8250	10.7350	21.94
D	0.1673	0.0883	0.1033	0.0874	25.1450	47.6700	2.6190	45.0510	93.57

In practice, it is believed that for mixtures with higher solute contents, the desired extraction percentage can be achieved by adopting mass transfer optimization strategies. Among them: an increase in the number of stages (contact and separation); an increase in the driving force of the process; favoring the flow of material of interest; increase in a concentration gradient etc.

4. Conclusions

The application of construction of a ternary phase diagram in the study the liquid-liquid extraction of the water/ethanoic acid/ethyl ethanoate system was quite satisfactory. The obtention of the equilibrium data of the ternary system made it possible an evaluation of the distribution and of the mutual solubility of the solute in the aqueous and organic phases. The determination of the composition of the extract and residue portions in the equilibrium of each mixture by of the tie-lines method allowed to examine the percentages of liquid-liquid extraction achieved by ethyl ethanoate. The acting of the solvent was evaluated by calculations of separation factors and percentage extraction, showing its good performance as an extractor solvent of ethanoic acid in the aqueous phase at room temperature and atmospheric pressure.

5. References

[1] García, N., Caballero, J. A., Economic and environmental assessment of alternatives to the extraction of acetic acid from water, Industrial & Engineering Chemistry Research 50 (2011) 10717-10729. https://doi.org/10.1021/ie201064x.

[2] IJmker, H. M., Gramblicka, M., Kersten, S. R. A., van der Ham, A. G. J., Schuur, B., Acetic acid extraction from aqueous solutions using fatty acids, Separation and Purification Technology 125 (2014) 256-263. https://doi.org/10.1016/j.seppur.2014.01.050.

[3] Pal, P., Nayak, J., Acetic acid production and purification: critical review towards process intensification, Separation & Purification Reviews 46 (1) (2017) 44-61. https://doi.org/10.1080/15422119.2016.1185017.

[4] Li, H., Wan, L., Chu, G., Tan, W., Liu, B., Qin, Y., Feng, Y., Sun, D., Fang, Y., (Liquid + liquid) extraction of phenols from aqueous solutions with cineole, Journal of Chemical Thermodynamics 107 (2017) 95-103. https://doi.org/10.1016/j.jct.2016.12.018.

[5] Wongsawaa, T., Hronec, M., Pancharoena, U., Phatanasri, S., Solubility and tie-line data for ternary aqueous mixtures of cyclopentanol with organic solvents at T = 298.2K: experiments and NRTL model, Fluid Phase Equilibria 379 (2014) 10-18. https://doi.org/10.1016/j.fluid.2014.07.011.

[6] Xu, D., Zhang, L., Gao, J., Pratik, D., Zhao L., Cui, Z., Liquid-liquid equilibrium for ternary systems of ethyl acetate/isopropyl acetate + 2,2,3,3-tetrafluoro-1-propanol + water at 298.15, 318.15 K, Journal of Chemical Thermodynamics 106 (2017) 218-227. https://doi.org/10.1016/j.jct.2016.12.006.

[7] Gilani, H. G., Gilani, A. G., Sangashekan, M., Tie-line data for the aqueous solutions of phenol with organic solvents at T = 298.2 K, Journal of Chemical Thermodynamics 58 (2013) 142-148. https://doi.org/10.1016/j.jct.2012.10.028.

[8] Lee, K. Y., Model to describe the binodal curve on a type 1 ternary phase diagram, Journal of Environmental Engineering 136 (6) (2010) 650-657. https://doi.org/10.1061/(ASCE)EE.1943-7870.0000196.

[9] Pontifícia Universidade Católica de Minas Gerais. Equilíbrio líquido-líquido para o sistema água/acetato de etila/ácido acético, PUC Minas, Belo Horizonte, 2017.

Eclética Química Journal, vol. 44, n. 3, 2019, 43-49
ISSN: 1678-4618
DOI: 10.26850/1678-4618eqj.v44.3.2019.p43-49

[10] Treybal, R. E., Mass-transfer operations, McGrall Hill Book Company, New York, 3rd ed., 1980.

[11] Yang, Z., Zhu, J., Wu, B., Chen, K., Ye, X., Liquid-Liquid Equilibrium of (Water + Pentane-2,4-dione + Ethyl Ethanoate) and (Water + Pentane-2,4-dione + Cyclohexane) at (298.15 and 313.15) K, Journal of Chemical & Engineering Data 55 (12) (2010) 5745-5750. https://doi.org/10.1021/je100704j.

[12] Cella, R. F., Mumbach, G. D., Andrade, K. L., Oliveira, P., Marangoni, C., Bolzan, A., Bernard, S., Machado, R. A. F., Polystyrene recycling processes by dissolution in ethyl acetate, Journal of Applied Polymer Science 135 (18) (2018). https://doi.org/10.1002/APP.46208.

Eclética Química Journal, vol. 44, n. 3, 2019, 43-49
ISSN: 1678-4618
DOI: 10.26850/1678-4618eqj.v44.3.2019.p43-49

Eclética Química Journal

Original article
iq.unesp.br/ecletica

| Vol. 44 | n. 3 | 2019 |

Solution of the Schrödinger equation with inversely quadratic Yukawa potential (IQYP) plus Kratzer-Fues (KFP) potential using the WKB quantum mechanical formalism

Benedict Iserom Ita, Hitler Louis+, Nelson Nzeata-Ibe

University of Calabar (Unical), Faculty of Physical Sciences, P.M.B 1115, Calabar, Cross River State, Nigeria.

+Corresponding author: Hitler Louis, email address: louismuzong@gmail.com

ARTICLE INFO

Article history:
Received: December 18, 2018
Accepted: February 25, 2019
Published: July 4, 2019

Keywords:
1. Schrödinger equation
2. inversely quadratic Yukawa potential
3. attractive Coulomb potential
4. Kratzer Fues potential
5. WKB approximation

ABSTRACT: The main objective of this research work is theoretical investigate the bound state solutions of the non-relativistic Schrödinger equation with a mixed potential composed of the Inversely Quadratic Yukawa/Attractive Coulomb potential plus a Modified Kratzer potential (IQYCKFP) by utilizing the Wentzel-Kramers-Brillouin (WKB) quantum theoretical formalism. The energy eigenvalues and its associated wave functions have successfully been obtained in sequel to certain diatomic molecules includes; HCL, HBr, LiH.

Bound State Solution of the Schrödinger Equation

$$E_{n\ell} = D_e - 2V_0\delta^2 - \frac{m(A+2D_e r_e - 2V_0\delta)^2 / 2\hbar^2}{\left[\left(n+\frac{1}{2}\right)+\sqrt{\left(\ell+\frac{1}{2}\right)^2 - \frac{2m}{\hbar^2}\left(V_0 - D_e r_e^2\right)}\right]^2}$$

1. Introduction

One of the interesting problems in quantum mechanics is to get exact solutions of the Schrödinger equation. To do this, a real potential is often selected to serve as the driving force of the energy eigenvalues and the eigenfunctions of the Schrödinger equation[1-3]. These state solutions reveal the particle dynamics in non-relativistic quantum mechanics[2]. Numerous researchers have investigated the bound states of the Schrödinger equation using variety of potentials and quantum formalism. Some of these potentials play critical roles in many fields of Physics such as Molecular Physics, Solid State and Chemical Physics[4]. The Manning-Rosen potential has been studied in-depth and have also been utilized in quantum systems and Yukawa potential, and its classes have been studied in Schrödinger formalism[5,6].

In this work, using the Wentzel, Kramers and Brillouin (WKB) quantum approximation, we shall investigate the bound state solutions of the Schrödinger equation using a combination of potentials known as the Inversely Quadratic Yukawa/Attractive Coulomb potential plus a Modified Kratzer potential (IQYCKFP).

2. The WKB Theoretical Approximation

In this section, we consider the quasiclassical solution of the Schrödinger's equation for the spherically symmetric potentials. Given the Schrödinger equation for a spherically symmetric potentials $V(r)$ of Equation 3 as

$$(-i\hbar)^2\left(\frac{\partial^2}{\partial r^2}+\frac{1}{r^2}\frac{\partial^2}{\partial\theta^2}+\frac{1}{r^2\sin^2\theta}\frac{\partial^2}{\partial\phi^2}\right)\psi(r,\theta,\phi) = \left[2m\left(E-V(r)\right)\right]\psi(r,\theta,\phi) \quad (1)$$

Eclética Química Journal, vol. 44, n. 3, 2019, 50-55
ISSN: 1678-4618
DOI: 10.26850/1678-4618eqj.v44.3.2019.p50-55

The total wave function in Equation 3 can be defined as

$$\psi(r,\theta,\phi) = [rR(r)]\left[\sqrt{sin\theta}\Theta(\theta)\Phi(\phi)\right] \quad (2)$$

And by decomposing the spherical wave function in Equation 1 using Equation 2 we obtain the following equations:

$$\left(-i\hbar\frac{\mathrm{d}}{\mathrm{dr}}\right)^2 R(r) = \left[2m\left(E - V(r)\right) - \frac{\vec{M}^2}{r^2}\right]R(r), \quad (3)$$

$$\left(-i\hbar\frac{\mathrm{d}}{\mathrm{d}\theta}\right)^2 \Theta(\theta) = \left[\vec{M}^2 - \frac{M_z^2}{\sin^2\theta}\right]\Theta(\theta), \quad (4)$$

$$\left(-i\hbar\frac{\mathrm{d}}{\mathrm{d}\phi}\right)^2 \Phi(\phi) = M_z^2\Phi(\phi) \quad (5)$$

where $\vec{M}^2$, M_z^2 are the constants of separation and, at the same time, integrals of motion. The squared angular momentum $\vec{M}^2 = \left(l+\frac{1}{2}\right)^2\hbar^2$.

Considering Equation 6, the leading order WKB quantization condition appropriate to Equation 3 is

$$\int_{r_1}^{r_2}\sqrt{P^2(r)}\,dr = \pi\hbar\left(n+\frac{1}{2}\right), \text{ n=0, 1, 2} \quad (6)$$

where r_2 & r_1 are the classical turning point known as the roots of the equation

$$P^2(r) = 2m\left(E - V(r)\right) - \frac{\left(l+\frac{1}{2}\right)^2\hbar^2}{r^2} = 0 \quad (7)$$

Equation 9 is the WKB quantization condition which is subject for discussion in the preceding section. Consider Equations 5-7 in the framework of the quasi-classical method, the solution of each of these equations in the leading $\hbar$ approximation can be written in the form

$$\Psi^{WKB}(r) = \frac{A}{\sqrt{P(r,\lambda)}}exp\left[\pm\frac{i}{\hbar}\int\sqrt{P^2(r)}\,dr\right] \quad (8)$$

3. Solutions of the Schrödinger Equation

The Wentzel, Kramers and Brillouin surmise has been of tremendous importance to physicist, chemist, mathematician as regards quantum mechanics in view of the fact that it gives approximate solutions to linear differential equations. The inversely quadratic Yukawa/attractive Coulomb plus Kratzer Fues potential can be expressed thus

$$V(r) = -\frac{1}{r^2}(V_0) + \frac{1}{r}(2V_0\delta - A) + (-2V_0)\delta^2 \text{ and } V(r) = D_e\left(\frac{r-r_e}{r}\right)^2 \quad (9)$$

The sum of these potentials can be written as

$$V(r) = \frac{2V_0\delta}{r} - \frac{A}{r} - \frac{V_0}{r^2} - 2V_0\delta^2 + D_e - \frac{2D_e r_e}{r} + \frac{D_e r_e^2}{r^2} \quad (10)$$

Eclética Química Journal, vol. 44, n. 3, 2019, 50-55
ISSN: 1678-4618
DOI: 10.26850/1678-4618eqj.v44.3.2019.p50-55

$$V_{eff\,(r)} = D_e - 2V_0\delta^2 + \frac{2V_0\delta}{r} - \frac{A}{r} - \frac{2D_e r_e}{r} - \frac{V_0}{r^2} + \frac{D_e r_e^2}{r^2} + \frac{\ell(\ell+1)\hbar^2}{2mr^2} \tag{11}$$

$$Q(r) = \sqrt{2m(E - V_{eff\,(r)})} \tag{12a}$$

Equation 12a stands for the classical formula for momentum.

$$\int_{ra}^{rb} Q(r)dr = \left(n + 1/2\right)\pi\hbar;\ \text{n=0, 1,2,3…} \tag{12b}$$

Upon, substituting Equations 11 and 12a into 12b i.e. the (WKB) we have

$$\int_{ra}^{rb} \sqrt{2m\left(E_{ne} - D_e + 2V_0\delta^2 - \frac{2V_0\delta}{r} + \frac{A}{r} + \frac{2D_e r_e}{r} + \frac{V_0}{r^2} - \frac{D_e r_e^2}{r^2} - \frac{\ell(\ell+1)\hbar^2}{2mr^2}\right)}dr = \left(n + 1/2\right)\pi\hbar$$

Factoring out $\sqrt{2m}$ (13)

$$\sqrt{2m}\int_{rA}^{rB} \sqrt{\left(E_{ne} - D_e + 2V_0\delta^2 - \frac{2V_0\delta}{r} + \frac{A}{r} + \frac{2D_e r_e}{r} + \frac{V_0}{r^2} - \frac{D_e r_e^2}{r^2} - \frac{\ell(\ell+1)\hbar^2}{2mr^2}\right)}dr = \left(n + 1/2\right)\pi\hbar \tag{14}$$

$$\sqrt{2m}\int_{rA}^{rB} \sqrt{\frac{1}{r^2}\left[\left(E_{ne} - D_e + 2V_0\delta^2\right)r^2 + \left(-2V_0\delta + A + 2D_e r_e\right)r - \left(D_e r_e^2 - V_0 + \frac{\ell(\ell+1)\hbar^2}{2m}\right)\right]}dr \tag{15}$$
$$= n + 1/2\,\pi\hbar$$

$$\sqrt{2m}\int_{rA}^{rB} \frac{1}{r}\sqrt{\left[\left(E_{ne} + 2V_0\delta^2 - D_e\right)r^2 + \left(A + 2D_e r_e - 2V_0\delta\right)r - \left(D_e r_e^2 - V_0 + \frac{\ell(\ell+1)\hbar^2}{2m}\right)\right]}dr \tag{16}$$
$$= \left(n + 1/2\right)\pi\hbar$$

$$\left.\begin{aligned} -A &= E_{ne} + 2V_0\delta^2 - D_e \\ M &= A + 2D_e r_e - 2V_0\delta \\ N &= D_e r_e^2 - V_0 + \frac{\ell(\ell+1)\hbar^2}{2m} \end{aligned}\right\}$$ where the negative sign on -(A) indicates a bound state.

Upon substituting the representations made into Equation 16 we have

$$\sqrt{2m}\int_{ra}^{rb} \frac{1}{r}\left(\sqrt{-\tilde{A}r^2 + Mr - N}\right)dr = \left(n + 1/2\right)\pi\hbar. \tag{17}$$

Eclética Química Journal, vol. 44, n. 3, 2019, 50-55
ISSN: 1678-4618
DOI: 10.26850/1678-4618eqj.v44.3.2019.p50-55

Factoring out $\sqrt{\tilde{A}}$, we have

$$\sqrt{2m\tilde{A}}\int_{ra}^{rb}\frac{1}{r}\left(\sqrt{-r^2+\frac{M}{\tilde{A}}r-\frac{N}{\tilde{A}}}\right)dr=\left(n+1/2\right)\pi\hbar. \tag{18}$$

x represent $\frac{M}{\tilde{A}}$ and y as $\frac{N}{\tilde{A}}$

$$\sqrt{2m\tilde{A}}\int_{ra}^{rb}\frac{1}{r}\left(\sqrt{-r^2+xr-y}\right)dr=\left(n+1/2\right)\pi\hbar. \tag{19}$$

$$\sqrt{2m\tilde{A}}\int_{ra}^{rb}\frac{1}{r}\sqrt{(r-r_a)(r_b-r)}dr=\left(n+1/2\right)\pi\hbar. \tag{20}$$

Where we obtain the classical turning points r_a and r_b from the terms inside the square roots as;

$$r_a=\frac{x-\sqrt{x^2-4y}}{2},\ r_b=\frac{x+\sqrt{x^2-4y}}{2} \qquad \text{N/N: } \left\{\begin{matrix} r_a+r_b=x \\ r_ar_b=y \end{matrix}\right\} \tag{21}$$

Recall

$$\int_{r_a}^{r_b}\frac{1}{r}\sqrt{(r-r_a)(r_b-r)}dr=\pi\left[\frac{1}{2}(r_a+r_b)-\sqrt{r_ar_b}\right] \tag{22}$$

$$\sqrt{2m\tilde{A}}\cdot\frac{\pi}{2}\left(x-2\sqrt{y}\right)=\left(n+1/2\right)\pi\hbar \tag{23}$$

$$\tilde{A}=\frac{2mM^2}{4\left[\hbar\left(n+1/2\right)+\sqrt{2mN}\right]^2} \tag{24}$$

Upon substituting the coefficients of M, N, $\tilde{A}$ *into* Equation 24 to obtain the energy eigenvalue.

$$-E_{ne}-2V_0\delta^2+D_e=\frac{2m(A+2D_er_e-2V_0\delta)^2}{4\left[\hbar\left(n+1/2\right)+\hbar\sqrt{\frac{2mD_er_e^2-2mV_0}{\hbar^2}+\ell(\ell+1)}\right]^2} \tag{25a}$$

Initiating the Langer correction term $\ell\left(\ell+1\right)\rightarrow\left(\ell+1/2\right)^2$

Eclética Química Journal, vol. 44, n. 3, 2019, 50-55
ISSN: 1678-4618
DOI: 10.26850/1678-4618eqj.v44.3.2019.p50-55

$$E_{ne} = D_e - 2V_0\delta^2 - \frac{m(A + 2D_e r_e - 2V_0\delta)^2 \Big/ 2\hbar^2}{\left[\left(n + 1/2\right) + \sqrt{\left(\ell + 1/2\right)^2 - \frac{2m}{\hbar^2}\left(V_0 - D_e r_e^2\right)}\right]^2} \tag{25b}$$

The above equation results in the bound state energy spectrum with respect to quantum numbers of a vibrating-rotating diatomic molecule subject to the (IQYCKFP) potential. Thus, its corresponding wave function is given as

$$R_{ne(r)} = N_{ne} r^{\left(-1/2 + \sqrt{\left(\ell + \frac{1}{2}\right)^2 + \frac{2m}{\hbar^2}(D_e r_e^2 - V_0)}\right)} e^{-r^2\left(\sqrt{\frac{m}{2\hbar^2}(D_e - E_{ne} - 2V_0\delta^2)}\right)}$$
$$F_1\left(-n; 1 + \sqrt{\left(\ell + 1/2\right)^2 + \frac{2m}{\hbar^2}\left(D_e r_e^2 - V_0\right)};\ \left(2\sqrt{\frac{m}{2\hbar^2}\left(D_e - E_{ne} - 2V_0\delta^2\right)}\right) r^2\right) \tag{26}$$

4. Discussion

Having obtained the Energy Eigen Value and its corresponding (ψ) using the WKB approach for the Schrödinger equation with the (IQYCKFP), we understood that if we set up parameters $D_e = 0,\ V_0 \neq 0$ and $A = Ze^2$

$$E_{ne} = -2V_0\delta^2 - \frac{m(A - 2V_0\delta)^2 \Big/ 2\hbar^2}{\left[n + 1/2 + \sqrt{\left(\ell + 1/2\right)^2 - \frac{2m}{\hbar^2}V_0}\right]^2} \tag{27}$$

5. Conclusions

It is much easy to show that Equation 19 has resulted to a bound state energy spectrum of a vibrating rotating diatomic molecule subject to the inversely quadratic Yukawa plus attractive coulomb potential.

Similarly, if $D_e \neq 0,\ V_0 = 0$ and $A \neq Ze^2 = 0$

$$E_{ne} = D_e - \frac{m(2D_e r_e)^2 \Big/ 2\hbar^2}{\left[\left(n + 1/2\right) + \sqrt{\left(\ell + 1/2\right)^2 + \frac{2m}{\hbar^2}\left(D_e r_e^2\right)}\right]^2} \tag{28}$$

Equation 28 results to a bound state energy spectrum subject to Kratzer Fues potential.

6. Acknowledgement

The authors are thankful to Professor Benedict I. Ita for the scientific encouragement leading to the success of this manuscript.

Eclética Química Journal, vol. 44, n. 3, 2019, 50-55
ISSN: 1678-4618
DOI: 10.26850/1678-4618eqj.v44.3.2019.p50-55

7. References

[1] Antia, A. D, Essien, I. E., Umoren, E. B., Eze, C. C., Approximate solution of the non-relativistic Schrödinger equation with inversely quadratic Yukawa plus Mobius square potential via parametric Nikiforov-Uvarov method, advances in Physics theories and application, 44 (2015) 1-13. https://iiste.org/Journals/index.php/APTA/article/view/23029/23549.

[2]Ita, B. I., Louis, H., Nzeata-Ibe, N., Ikeuba, A., Ozioma, A. U., Thomas, M. O., Pigweh, A. I., Michael, M. O., Approximate $\boldsymbol{l}$-states solutions to the Schrödinger equation with Manning-Rosen plus Hellmann potential via WKB approximation scheme, Sri Lankan Journal of Physics 19 (1) (2018) 37-45. https://doi.org/10.4038/sljp.v19i1.8050.

[3] Onate, C. A., Adebimpe, O., Lukman, A. F., Adama, I. J., Okoro, J. O., Davids, E. O., Approximate eigensolutions of the attractive potential via parametric Nikiforov-Uvarov method, Heliyon 4 (11) (2018). https://doi.org/10.1016/j.heliyon.2018.e00977.

[4] Hitler, L., Iserom, I. B., Tchoua, P., Ettah, A. A., Bound state solutions of the Klein-Gordon equation for the more general exponential screened Coulomb potential plus Yukawa (MGESCY) potential using Nikiforov-Uvarov method, J. Phys. Math. 9 (1) (2018). https://doi.org/10.4172/2090-0902.1000261.

[5] Ikot, A. N., Hassanabadi, H., Maghsoodi, E., Zarrinkamar, S., Relativistic symmetries of Hulthén potential incorporated with generalized tensor interactions, advances in high energy physics 2013 (2013) 1-10. https://doi.org/10.1155/2013/910419.

[6] Ita, B. I., Louis, H., Akakuru, O. U., Magu, T. O., Joseph, I., Tchoua, P., Amos, P. I., Effiong, I., Nzeata, N. A., Bound state solutions of the Schrödinger equation for the more general exponential screened Coulomb potential plus Yukawa (MGESCY) potential using Nikiforov-Uvarov method, Journal of Quantum Information Science 8 (1) (2018) 24-45. https://doi.org/10.4236/jqis.2018.81003.

Eclética Química Journal, vol. 44, n. 3, 2019, 50-55
ISSN: 1678-4618
DOI: 10.26850/1678-4618eqj.v44.3.2019.p50-55